Monthly Notices
of the
ROYAL ASTRONOMICAL SOCIETY

MNRAS **472,** 4173–4192 (2017)
Advance Access publication 2017 September 4

doi:10.1093/mnras/stx2243

Multiband photometry and spectroscopy of an all-sky sample of bright white dwarfs

R. Raddi,[1]★ N. P. Gentile Fusillo,[1] A. F. Pala,[1] J. J. Hermes,[2]† B. T. Gänsicke,[1] P. Chote,[1] M. A. Hollands,[1] A. Henden,[3] S. Catalán,[4] S. Geier,[5] D. Koester,[6] U. Munari,[7] R. Napiwotzki[8] and P.-E. Tremblay[1]

[1]*Department of Physics, University of Warwick, Gibbet Hill Road, Coventry CV4 7AL, UK*
[2]*Department of Physics and Astronomy, University of North Carolina, Chapel Hill, NC 27599, USA*
[3]*AAVSO, 49 Bay State Rd Cambridge, MA 02138, USA*
[4]*Centre for Astronomy, National University of Ireland Galway, Galway, Ireland*
[5]*Institute for Astronomy and Astrophysics, Eberhard Karls University, Sand 1, D-72076 Tübingen, Germany*
[6]*Institut für Theoretische Physik und Astrophysik, Universität Kiel, D-24098 Kiel, Germany*
[7]*INAF–Astronomical Observatory of Padova, I-36012 Asiago (VI), Italy*
[8]*Centre for Astrophysics Research, STRI, University of Hertfordshire, College Lane, Hatfield AL10 9AB, UK*

Accepted 2017 August 28. Received 2017 August 28; in original form 2017 February 27

ABSTRACT

The upcoming NASA *Transiting Exoplanet Survey Satellite* (*TESS*) will obtain space-based uninterrupted light curves for a large sample of bright white dwarfs distributed across the entire sky, providing a very rich resource for asteroseismological studies and the search for transits from planetary debris. We have compiled an all-sky catalogue of ultraviolet, optical and infrared photometry as well as proper motions, which we propose as an essential tool for the preliminary identification and characterization of potential targets. We present data for 1864 known white dwarfs and 305 high-probability white dwarf candidates brighter than 17 mag. We describe the spectroscopic follow-up of 135 stars, of which 82 are white dwarfs and 25 are hot subdwarfs. The new confirmed stars include six pulsating white dwarf candidates (ZZ Cetis), and nine white dwarf binaries with a cool main-sequence companion. We identify one star with a spectroscopic distance of only 25 pc from the Sun. Around the time *TESS* is launched, we foresee that all white dwarfs in this sample will have trigonometric parallaxes measured by the ESA *Gaia* mission next year.

Key words: catalogues – binaries: spectroscopic – binaries: visual – subdwarfs – white dwarfs.

1 INTRODUCTION

White dwarfs are the final evolutionary stage for the vast majority of single stars. Characterized by long, steady cooling rates, white dwarfs can be used to infer properties of the Milky Way like the star formation history (Tremblay et al. 2014), the age of the disc (Winget et al. 1987; Oswalt et al. 1996) or their contribution to baryonic dark matter (Reid, Sahu & Hawley 2001; Pauli et al. 2003).

Asteroseismology is a powerful tool for probing the internal structure of white dwarfs, through the study of multiperiodic variability that occurs during short-lived instability phases on the white dwarf cooling sequence (Fontaine & Brassard 2008; Winget & Kepler 2008; Althaus et al. 2010). Over the last few years, the NASA *Kepler* mission (Borucki et al. 2010) and its re-purposed two-wheeled *K2* mission (Howell et al. 2014) have enabled high-precision asteroseismology of white dwarfs (Hermes et al. 2011; Østensen et al. 2011; Greiss et al. 2016). Its successor, the NASA *Transiting Exoplanet Survey Satellite* (*TESS*; Ricker et al. 2015), will acquire all-sky times-series photometry for at least 2 yr, searching for exoplanet transits and enabling asteroseismology for many classes of stars (Campante et al. 2016). Roughly 200 000 selected targets, including bright white dwarfs, may be observed with 2-min cadence. Full-frame images will be taken every 30 min. The mission will survey areas of sky with 1-month to 1-yr coverage, depending on their ecliptic latitudes.

TESS is poised to return improved statistics building upon the original *Kepler* mission and its ongoing *K2* reincarnation. In particular, the large sky coverage of *TESS* will be excellent for the discovery of rare phenomena of which *Kepler* has so far provided us with few, or even unique examples, e.g. the first direct detection of

★E-mail: r.raddi@warwick.ac.uk
†Hubble Fellow.

a disintegrating asteroid at a white dwarf (Vanderburg et al. 2015) or the identification of stochastic outbursts in cool pulsating white dwarfs (Bell et al. 2015, 2016; Hermes et al. 2015). *TESS* is expected to be launched in 2018 March–July, which is just before or at the same time of the second data release of the ESA *Gaia* mission (DR2; Gaia Collaboration 2016a; Lindegren et al. 2016). Therefore, the need of an all-sky target list of bright white dwarfs is extremely urgent, especially for the southern ecliptic hemisphere, which will not have the benefit of *Gaia* selection. Bright white dwarfs can also be monitored by upcoming photometric missions, such as Evryscope (Law et al. 2015) or the Next Generation Transit Survey (NGTS; West et al. 2016).

Traditionally, the identification of white dwarfs relies on their blue colours and relatively large proper motions. The availability of accurate digital photometry and astrometry has greatly improved the efficiency of white dwarf selection (e.g. Kawka & Vennes 2006; Kilic et al. 2006; Limoges, Lépine & Bergeron 2013; Gentile Fusillo, Gänsicke & Greiss 2015; Raddi et al. 2016; Gentile Fusillo et al. 2017). Numerous efforts have been undertaken to improve the identification and characterization of bright and nearby white dwarfs (Sion et al. 2014; Holberg et al. 2016), not only through spectroscopy and photometry (Giammichele, Bergeron & Dufour 2012), but also including trigonometric parallaxes (e.g. DENSE project;[1] Subasavage et al. 2009). So far, the white dwarf census is strongly biased towards the Northern hemisphere, which Limoges, Bergeron & Lépine (2015) estimate to be 78 per cent complete at 40 pc.

In the following sections, we describe a collection of proper motions and multiband all-sky photometry for potential *TESS* white dwarf targets. Out of 2990 known white dwarfs brighter than 17 mag, we re-identify 1864 stars, i.e. 62 per cent of the total. We discuss the properties of the sample and its completeness via comparison with catalogues of spectroscopically confirmed white dwarfs and the Lowell Observatory proper motion survey (Giclas, Burnham & Thomas 1980, GD sample). We present photometry and proper motions for 305 new high-probability white dwarf candidates, and 33 white dwarf candidates in the GD sample. In the last part of the paper, we discuss the properties of 82 white dwarfs and 25 hot subdwarfs for which we acquired follow-up spectroscopy.

2 THE DATA

The photometric identification of white dwarfs hotter than $\simeq 6000$ K is very effective with colours sampling the flux across the Balmer jump, e.g. *ugr* photometry of the Sloan Digital Sky Survey (SDSS; Girven et al. 2011). Currently, there is no single all-sky survey covering this spectral region for magnitudes brighter than 17th magnitude. A useful alternative is offered by the combination of far- and near-ultraviolet photometry (FUV and NUV bands, centred at 1540 and 2270 Å, respectively) from the *Galaxy Evolution Explorer* (*GALEX*; Morrissey et al. 2007) with optical photometry from the AAVSO Photometric All-Sky Survey (APASS; Henden & Munari 2014) in the Johnson *BV* and Sloan $g'r'i'$ passbands.

Bianchi et al. (2011) discussed the properties of hybrid colour–colour diagrams of *GALEX* and SDSS photometry showing their potential at separating classes of Galactic and extragalactic sources. Limoges et al. (2013) have used similar colour combinations to select white dwarfs candidates in the Northern hemisphere from *GALEX*, SDSS, *Hipparcos* (van Leeuwen 2007) and *Tycho-2* (Høg et al. 2000), using proper motions from SUPERBLINK (Lépine & Shara 2005). In the work described here, we used the PPMXL catalogue that includes positions and proper motions for 900 million stars derived from USNO-B 1.0 (Monet et al. 2003) and the Two-Micron All-Sky Survey (2MASS; Skrutskie et al. 2006) astrometry in the International Coordinate Reference System. In addition to the ultraviolet, optical and near-infrared photometry, we also added mid-infrared data from the *Wide-field Infrared Survey Explorer* (*WISE*; Wright et al. 2010). In Table 1, we list the wavelength coverage of the used set of filters.

Table 1. Photometric bands used in this work. Refer to the Spanish Virtual Observatory web pages[a] for the definition of effective wavelength and width, $\lambda_{\rm eff}$ and $W_{\rm eff}$, respectively.

Survey	Filters	$\lambda_{\rm eff}$ (nm)	$W_{\rm eff}$ (nm)
GALEX	FUV	154	25
	NUV	227	73
APASS	B	430	84
	g'	464	116
	V	539	87
	r'	612	111
	i'	744	104
2MASS	J	1235	162
	H	1662	251
	$K_{\rm s}$	2619	162
WISE	$W1$	3353	663
	$W2$	4602	1042

[a] http://svo2.cab.inta-csic.es/theory/vosa4/

2.1 The reference catalogue: APASS

APASS data release 9 (DR9; Henden et al. 2016) contains ≈61 million objects in the 10th–17th magnitude range. The survey uses two pairs of 20-cm twin telescopes: two in the north at Dark Ridge Observatory in New Mexico, and two in the south at the Cerro Tololo Inter-American Observatory. This set-up allows automated, essentially simultaneous observations in the *BV* and $g'r'i'$ bands. The pixel scale at detectors is 2.57 arcsec, and photometry is extracted using a 15-arcsec aperture in the north and 20 arcsec in the south, due to differences in the focusing of telescopes. APASS DR9 is suggested to be currently complete down to $V = 16$, and it is expected to be complete down to $V = 17$ at the end of the survey. The bright limit of APASS is of little concern here, as there are only two known white dwarfs brighter than 10 mag (i.e. Sirius B and 40 Eri B; see next section). The astrometric accuracy is 0.15 arcsec and the photometric accuracy is 0.02 mag at 15 mag (Munari et al. 2014). The release notes[2] suggest a careful use of APASS photometry in crowded areas, where the photometry extraction algorithm suffers from blending. Furthermore, the most recent measures of B, g' magnitudes in the north are known to carry large random errors, due to a technical problem with the detectors. Nevertheless, APASS photometry was shown to be sufficiently accurate for tying other deeper surveys on to an absolute flux scale (e.g. Barentsen et al. 2014; Drew et al. 2014; Shanks et al. 2015).

Duplicated entries are present in APASS DR9 due to merging issues at the detector corners and for high proper motion objects. Thus, we generated a reduced data set of unique sources within a separation of <1.25 arcsec, which corresponds to half a pixel of APASS detectors. When more than one photometric value is identified in this internal cross-match process, we adopted the brightest

[1] http://www.DenseProject.com

[2] https://www.aavso.org/apass

Table 2. Results of the all-sky cross-match.

Survey	No. of objects
APASS DR9	61 176 401
APASS DR9 unique	58 756 366
APASS + *GALEX* (FUV and NUV)	19 037 824
APASS + *GALEX* NUV unique	15 558 208
APASS + PPMXL	44 290 772
APASS + 2MASS	42 901 844
APASS + *WISE*	43 179 834

detection as suggested in the APASS DR9 release notes. The so-defined unique list of APASS sources contained a little less than 59 million objects.

2.2 Matching with PPMXL, *GALEX* and *WISE*

To cross-correlate APASS with *GALEX* and *WISE* detections, we needed to account for stellar proper motions. Thus, we first queried the PPMXL data base via Table Access Protocol (TAP), using the Starlink Tables Infrastructure Library Tool Set (STILTS; Taylor 2006). The query was run by uploading the entire unique APASS data set to the online service,[3] split in to chunks of 100 000 rows each. For each APASS source, we identified all the PPMXL objects within 45 arcsec. Then, assuming epoch 2013.0 for the APASS DR9 coordinates, we forward-propagated the coordinates of PPMXL sources using their proper motions. Finally, we identified good matches by selecting objects that fall within 2 arcsec from the APASS sources. The APASS-PPMXL cross-match produced ≈45 million objects.

The next step was to cross-match the APASS-PPMXL sources with the *GALEX* DR6+DR7 data base,[4] accessing the Catalog Archive Server Jobs System (CasJobs) via Simple Object Access Protocol. In CasJobs, we first queried the PhotoObjAll table to search for all the nearby sources within 45 arcsec from the position of our APASS-PPMXL sources; then, we identified the corresponding observing dates in the photoExtract table to propagate APASS coordinates to the corresponding *GALEX* epochs, again using the PPMXL proper motions. The cross-match with *GALEX* reduced further the number of APASS-PPMXL sources with proper motions and NUV photometry, leaving ≈19 million detections (i.e. about 15 million unique sources).

As last step, we cross-matched the APASS-PPMXL source list with *WISE* via TAP. Again, we shifted the APASS coordinates backwards in time by taking into account the epoch difference between APASS and *WISE*.

In Table 2, we summarize the results of the cross-match procedure. It is important to stress here that we used the APASS-PPMXL-*GALEX* (APG, hereafter) cross-match to characterize and identify most of the white dwarfs described in this paper. We used *WISE* photometry to probe for infrared excess, e.g. the binary systems discussed in Section 6.5.

To visualize the cross-match procedure, we display in Fig. 1 the identification of a newly confirmed white dwarf, J0515+5021 (GD 289). We note the star's significant proper motion across different epochs when the considered set of images was taken.

[3] PPMXL is hosted by the German Astronomical Virtual Observatory data centre at http://dc.zah.uni-heidelberg.de/.

[4] *GALEX* DR6+DR7 is hosted by the Mikulski Archive for Space Telescopes (MAST) at http://galex.stsci.edu/GR6/.

3 ASSESSING THE CROSS-MATCH

To verify the completeness of the APG cross-match, we compared the data to a set of catalogues from the literature. Our first comparison is done against the GD sample (Giclas et al. 1980) that contains blue stellar objects with proper motions of $\lesssim 0.20$ arcsec yr^{-1} and includes 311 previously known white dwarfs. In this work, we have confirmed 12 new GD stars as white dwarfs.

During this operation, we visually inspected finding charts to confirm our re-identifications. We download cut-out images from the NASA SkyView service,[5] i.e. blue and red frames of the STScI Digitized Sky Survey,[6] 2MASS and *GALEX*, and for known white dwarfs we used finding charts available at the DENSE web pages, or those made available by Tom Marsh.[7]

We make all the photometry and proper motions for the re-identified stars available on VizieR (hosted by the Strasbourg astronomical Data Center, CDS; Wenger et al. 2000). Table A1 describes the columns that are included in the online tables.

3.1 The GD sample

The catalogue of blue stars from the Lowell Observatory proper motion survey contains 1710 unique objects. For this test, we used the list of coordinates and magnitudes that is available on VizieR (catalogue ID, II/299); these quantities are an updated collection of data from other surveys and not just from the original work. Through our cross-match described above, we successfully retrieved APASS photometry, PPMXL proper motions and *GALEX* photometry for 1479, 1455 and 1175 stars, respectively. Of these stars, we re-identify APASS photometry for 260 white dwarfs. In Fig. 2, the distribution of these magnitudes is compared to those from the GD catalogue as available on VizieR. In Fig. 2, we also display the distribution of PPMXL proper motions (μ) and angular separations between the APASS coordinates and those listed in VizieR. In the bottom-left panel of Fig. 2, we display the difference between the APASS V magnitudes plotted against the angular separations (APASS – VizieR coordinates). We measure a scatter of ± 0.15 mag around the zero. Five white dwarfs are at more than 5σ from the zero: GD 123, which has an M-dwarf companion; GD 167, for which the V-band photometry recorded in VizieR is ≈2 mag brighter than those measured in other bands available on SIMBAD (also hosted by CDS); GD 230, GD 272 and GD 546, for which we suspect the APASS photometry to be blended with nearby objects. In the bottom-right panel of Fig. 2, we display the correlation between PPMXL proper motions and angular separations. The majority of GD stars follow a linear trend, which is more evident for the known white dwarfs in the sample. After inspecting finding charts for these stars, we note that most of the scatter appears to be due to the limited accuracy of the reference positions that are listed in VizieR. The most discrepant white dwarfs, GD 230 (with an angular separation of 9 arcsec, off-scale in Fig. 2), is likely blended with nearby stars.

We inspected the literature on GD stars available through SIMBAD and divided them into six groups: white dwarfs, white dwarf candidates, subdwarfs, stars, unknown objects and QSOs. More than half of the GD stars have very little information available (i.e. no classification in the references) or no SIMBAD entry at all. In Fig. 3, we display the colour–colour and reduced proper motion diagrams of stars with APG data (the reduced proper motion is defined

[5] http://skyview.gsfc.nasa.gov/

[6] https://archive.stsci.edu/cgi-bin/dss_form

[7] http://deneb.astro.warwick.ac.uk/phsaap/wdcharts/

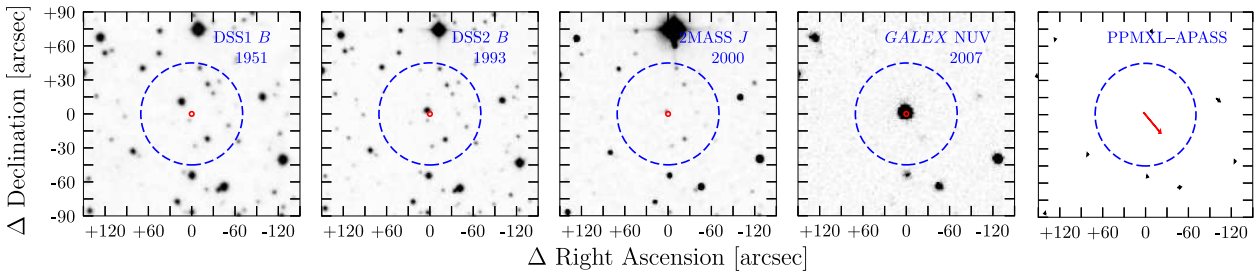

Figure 1. In the first four panels, we show the evolving position of the newly confirmed white dwarf J0515+5021 (GD 289). From left to right we display the cut-outs from the POSS-I and POSS-II blue plates, and the 2MASS *J* and *GALEX* NUV images. The rightmost panel displays the PPMXL proper motion vector (in arcsec yr^{-1}, multiplied by 100 to improve the visualization). In each panel, we plot the large cone-search of 45 arcsec used to identify objects with large proper motions (in blue) and a 2-arcsec circle for the cross-match at the APASS position (in red).

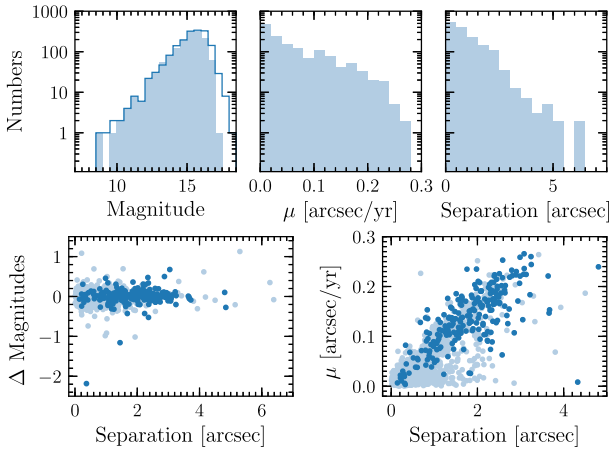

Figure 2. Assessment of the APG cross-match for the GD sample. *Top*: solid histograms represent the APASS *V*-band magnitudes, proper motions and angular separations between APASS coordinates and those available in VizieR. The step histograms represent the *V*-band magnitudes available on VizieR. *Bottom*: on the left, the differences between APASS magnitudes and those from the literature are plotted against the angular separation; on the right, we show the correlation between PPMXL proper motions, plotted against the angular separations. We use dark points to represent known white dwarfs and light coloured points for non-white dwarf sources.

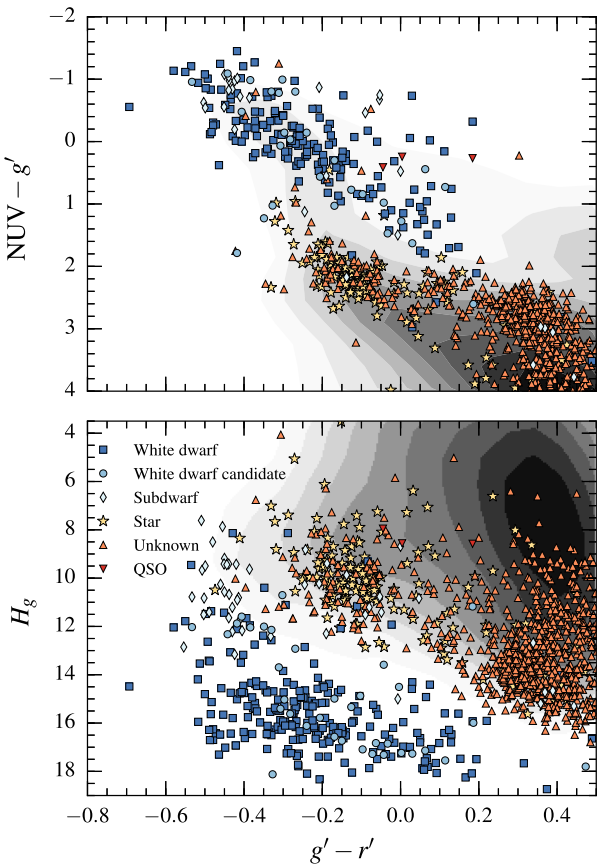

Figure 3. Colour–colour (top) and reduced proper motion (bottom) diagrams of the GD sample. The dark coloured contours in both panels represent the colour distribution of the field population, as inferred from our all-sky cross-match. The object classification is based on the information available from SIMBAD (see text). *Top*: white dwarf cooling sequences ($\log g = 7.0$–9.5 in 0.5 dex steps) and the main sequence are plotted for reference; both have been determined by convolving Koester (2010) synthetic spectra and Pickles (1998) spectra with the filter transmission profiles, respectively. *Bottom*: solid curves representing the expected reduced proper motions for $\log g = 8$ disc white dwarfs are plotted at three distinct values of tangential velocities, $V_T = 20$, 40 and 150 km s^{-1}. The curves follow the relation: $H_g = g' + 5 \times \log V_T - 3.379$.

as $H_g = g' + 5 + 5 \times \log \mu$, with the proper motion, μ, given in arcsec yr^{-1}). We note that confirmed white dwarfs and hot subdwarfs mostly separate from the main group of other stellar objects. Based on the colours, reduced-proper motions and the information available in SIMBAD, we identify 46-candidate white dwarfs, of which we observed 13 spectroscopically. In the GD sample, there are about 1100 objects with little or no information on SIMBAD, which have colours and proper motions that are compatible with those of main-sequence stars.

3.2 White dwarf samples

As seen from the previous test, the re-identification of known objects may present some issues due to the poor accuracy of reference positions. This can be accentuated for bright white dwarfs, because their coordinates were traditionally recorded in equinox B1950.0 with an accuracy of the order of 1 arcmin (e.g. McCook & Sion 1999) and possess on average large proper motions. With the advance of technology, higher accuracy is required, and there is an ongoing effort for updating the astrometry and proper motions of known white dwarfs, e.g. on SIMBAD and the Montréal White Dwarf Database (MWDD; Dufour et al. 2017).

To assess the completeness of the APG cross-match with respect to well-studied white dwarfs, we took into consideration five

spectroscopic catalogues that include about 2/3 of the spectroscopically confirmed white dwarfs within the APASS magnitude range. These are as follows: (i) the 25-pc sample (analysed by Sion et al. 2014); (ii) hydrogen (DA) and helium (DB/DBA) white dwarfs from the European Southern Observatory (ESO) supernovae Ia progenitor survey (SPY; Voss et al. 2007; Koester et al. 2009, respectively); (iii) DA and DB white dwarfs analysed by the Montréal group (to be distinguished from the MWDD, which contains a large fraction of the spectroscopically confirmed white dwarfs; Giannas et al. 2010; Bergeron et al. 2011); (iv) a bright selection ($g \leq 17$) of white dwarf plus main-sequence binaries (WD+MS) from SDSS (Rebassa-Mansergas et al. 2012). Covering most of the sky with Galactic latitudes of $|b| > 30$ deg, these catalogues allow for a semi-independent assessment of the photometric, proper motion and on-sky completeness of our APG data set. We note that for each catalogue we used the coordinates available online through VizieR or SIMBAD. Given that the accuracy of positions may be different in each catalogue, this can lead to possible mismatches and/or to non-identifications even for objects that are in more than one of the considered catalogues. When assessing the global-completeness, we took into account the unique objects across the catalogues.

3.2.1 *The local 25-pc sample*

For this comparison, we use the list of Sion et al. (2014), which contains 223 white dwarfs. We identify APASS matches for 169 stars. The unmatched objects include Sirius B or Procyon B, which are outshined by their bright main-sequence companions. In the top and bottom panels of Fig. 4, we display the comparison between APASS V photometry and data available on SIMBAD for the Sion et al. (2014) white dwarfs in the same band. For this sample, we measure a mean difference of ± 0.35 mag. Most of the outliers are due to contamination from nearby sources. We note that our cross-match becomes increasingly incomplete below 16.5 mag, and we do not retrieve any of the white dwarfs fainter than 17 mag (5 per cent of the total). The brightest white dwarf we re-identify is 40 Eri B (APASS $V = 9.3$).

The completeness of the cross-match with the Sion et al. (2014) sample is reduced to 116 white dwarfs when we consider PPMXL proper motions. The highest proper motion we retrieve is 1.25 arcsec yr^{-1} for WD 2248+293. From Fig. 4, we note that we are about 60 per cent complete for white dwarfs with proper motions $\leq$1 arcsec yr^{-1}.

In the top-right panel of Fig. 4, we present the distribution of angular separations between APASS and SIMBAD coordinates for the Sion et al. (2014) white dwarfs. 40 Eri B is the star with the largest angular separation (52 arcsec). We do not plot WD 0727+482A (with an angular separation of 90 arcsec, off-scale in Fig. 4), for which SIMBAD lists the coordinates of the companion.

In the bottom-right panel of Fig. 4, we display the correlation between angular separations (APASS – SIMBAD coordinates) and the proper motions. First, we note that the correlation follows closely a linear trend. Secondly, we fail to retrieve proper motions for stars with separations that are larger than 20 arcsec. Most of these objects move faster than 1.5 arcsec yr^{-1}. The lowest point not aligning with the others is WD 0108+277, the astrometry of which may be affected by the presence of a nearby background source (Farihi, Becklin & Zuckerman 2005; Holberg et al. 2016).

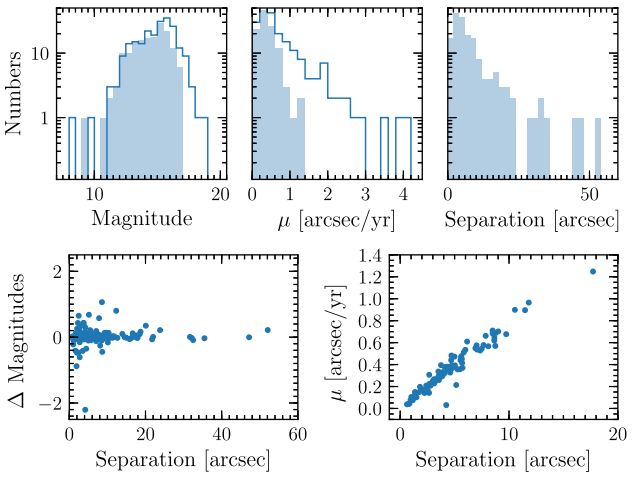

Figure 4. Assessment of the APG cross-match for white dwarfs in the 25-pc sample. Refer to Fig. 2 for a description of each panel.

3.2.2 *White dwarfs from the SPY project*

SPY was an ESO spectroscopic survey that targeted bright white dwarfs ($B \leq 16.5$) south of $\delta = +25$ deg (Napiwotzki et al. 2003). We tested the completeness of APASS on the DA and DB/DBA white dwarf catalogues published by Koester et al. (2009) and Voss et al. (2007), respectively. We re-identified 575 of the 669 DA white dwarfs, and 62 of the 69 DB/DBA white dwarfs from SPY. The comparison between APASS magnitudes and those available in the literature is shown in the left-hand panels of Fig. 5.

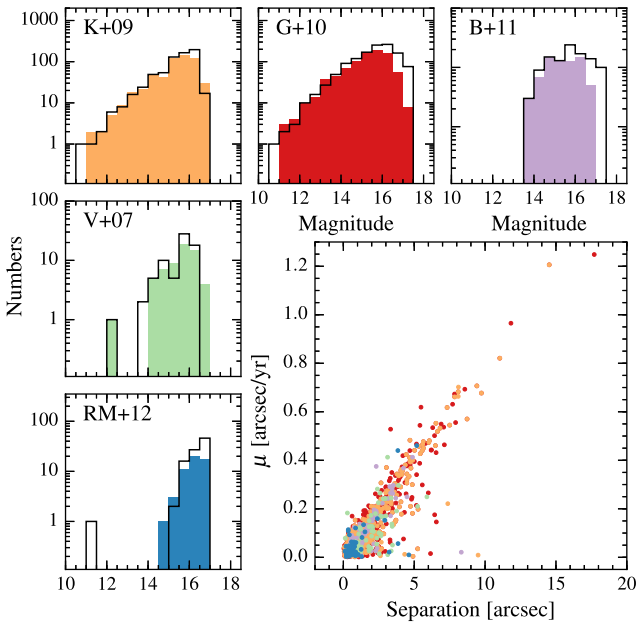

Figure 5. Validation of the APASS-PPMXL cross-match. The coloured histogram bars represent APASS magnitude distributions (V or g', depending on the subsample considered) for the five white dwarf catalogues we used as reference: K+09: Koester et al. (2009); V+07: Voss et al. (2007); G+10: Gianninas et al. (2010); B+11: Bergeron et al. (2011); RM+12: Rebassa-Mansergas et al. (2012). The black outline histograms represent the magnitude distributions of the known white dwarfs as retrieved from the literature. In the bottom-right panel, we plot the PPMXL proper motions against the angular separations between APASS coordinates and the positions available on VizieR/SIMBAD. Symbols are colour-coded with the same colours used of the histogram bars.

Table 3. Summary of the comparison between the APG cross-match with stars from the literature.

Catalogue	No. of objects	APASS	PPMXL	*GALEX* NUV	Reference
GD sample (all objects)	1710	1479	1455	1175	Giclas et al. (1980)
GD sample (confirmed white dwarfs)	323	260	246	174	
25 pc	223	169	116	40	Sion et al. (2014)
SPY DA	669	575	547	394	Koester et al. (2009)
SPY DB/DBA	69	62	59	37	Voss et al. (2007)
Montréal DA	1265	889	822	546	Gianninas et al. (2010)
Montréal DB/DBA	108	72	70	48	Bergeron et al. (2011)
WD+MS	92	55	54	39	Rebassa-Mansergas et al. (2012)
Total white dwarfs	1931	1388	1271	840	

We retrieved PPMXL proper motions for 547 DA and 59 DB/DBA white dwarfs. On average, proper motions of these stars are smaller in comparison with those of white dwarfs in the local sample, and therefore we have a higher success rate in re-identifying these stars through our selection method. In the bottom-right corner of Fig. 5, we display the correlation between PPMXL proper motions and angular separations between APASS and Vizier coordinates for the SPY sample. In the same panel, we plot also white dwarfs from the other samples discussed next. Proper motion and angular separations correlate well as found above for the Sion et al. (2014) sample. Just a few objects (e.g. WD 1334−678, WD 1943+163, WD 2029+183 and WD2157+161), which are blended with nearby stars may have inaccurate positions and/or proper motions.

3.2.3 *DA and DB white dwarfs analysed by the Montréal group*

These two white dwarf samples overlap to some degree with SPY, and consist of 1265 DA (Gianninas et al. 2010) and 108 DB/DBA white dwarfs (Bergeron et al. 2011). The relevant differences with the SPY sample are their spatial distribution that extends to the Northern hemisphere and a fainter limiting magnitude (≈17.5 mag). We identified APASS photometry for 889 DA and 72 DB/DBA white dwarfs. The magnitude distributions of both samples are displayed in the top-right panels of Fig. 5. We note that the completeness starts decreasing for stars that are fainter than 16.5 mag. In the bottom-right panel of Fig. 5, we find a good correlation between proper motions and angular separations also for these stars; like before, a few discrepant objects (e.g. WD 0927−173 or WD 1545+244) are close to nearby sources that cause less accurate measures of proper motions or positions.

3.2.4 *White dwarf plus main-sequence star binaries*

Rebassa-Mansergas et al. (2012) have produced the so far largest catalogue of WD+MS binaries[8] from SDSS, which has been recently updated to the data releases 9 and 12 (Rebassa-Mansergas et al. 2016). We selected a sample of 92 binaries with $g' \leq 17$, re-identifying APASS and PPMXL data for 55 and 54 of them, respectively. The magnitude distribution of the sample is displayed in the bottom-left corner of Fig. 5, while in the bottom-right panel we add the corresponding data points to the comparison between PPMXL proper motions and coordinate separations.

[8] http://www.sdss-WDMS.org/

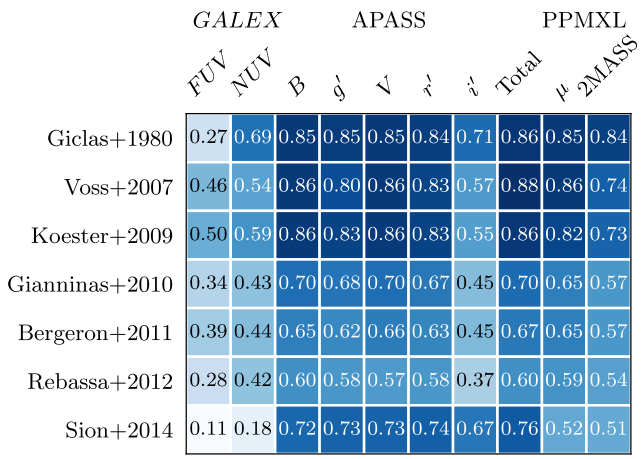

Figure 6. Completeness of the data set, expressed as fraction of the number of stars retrieved with respect to the total number of objects in the corresponding sample.

3.3 Completeness

Table 3 summarizes the tests of our combined APG catalogues. The completeness of the cross-match depends on the intrinsic properties of the different test cases, e.g. the magnitude limits and accuracy of positions. In total, we have retrieved APASS photometry for 1388 white dwarfs out of a sample of 1931 stars (72 per cent). We note that that the median magnitude of the white dwarfs for which we do not retrieve APASS data is $V \approx 16.5$, below which we are about 80 per cent complete. The completeness with respect to PPMXL and *GALEX* photometry is 66 and 43 per cent, respectively. A more detailed breakdown into survey passbands is displayed in Fig. 6, for the spectroscopic catalogues considered earlier.

In Fig. 7, we display the spatial distributions of the white dwarfs discussed in the previous sections. We checked for spatial clustering of the white dwarfs we could not re-identify. Most of the unidentified white dwarfs that were not recovered in our merged APG catalogue are in the Montréal sample and are located along a strip stretching from $\alpha = +0$–5 h and $\delta = -30, +15$ deg to $\alpha = 8$–15 h and $\delta = +30, +40$ deg. Some of them are from the Kiso survey (Limoges & Bergeron 2010, and references therein), which overlaps with the fainter end of APASS. We also note the traditional deficit of white dwarfs at low Galactic latitudes that is common to all the known samples of white dwarfs. At low latitudes, there is also no *GALEX* photometry, mainly due to the satellite avoiding

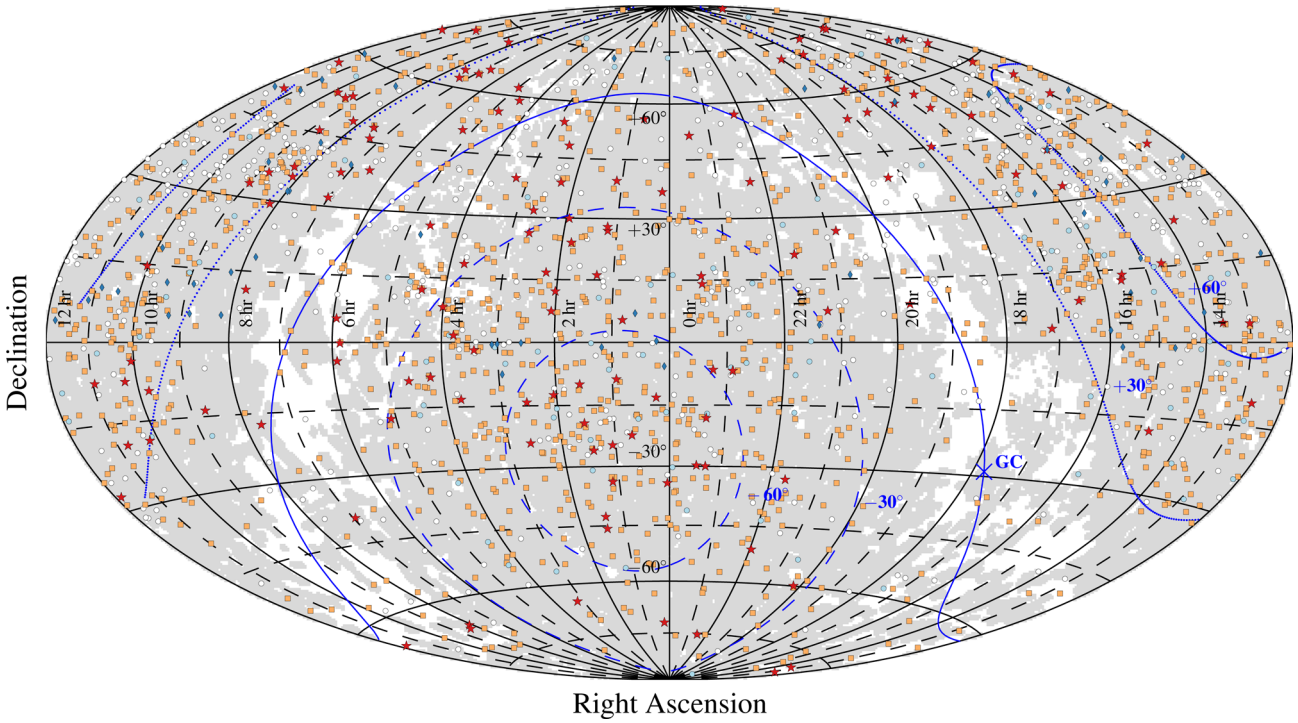

Figure 7. Spatial distribution in equatorial coordinates of the known white dwarfs from the literature discussed here. Coloured symbols are used for the objects we re-identify in our multiband photometric data set (squares: DA white dwarfs; circles: DB/DBA white dwarfs; diamonds: WD+MS; stars: 25-pc sample). White symbols correspond to white dwarfs with no APASS cross-match. The light grey-shaded area delimits the sky coverage of *GALEX*. Iso-Galactic latitude curves are overplotted in blue.

bright stars and crowded areas in the Galactic plane (note the white areas in Fig. 7).

Finally, we confirmed our results by checking all the remaining white dwarfs (where we define white dwarfs as objects with $\log g \geq 6$) in the MWDD and SDSS (Kleinman et al. 2013; Gentile Fusillo et al. 2015; Kepler et al. 2015, 2016), that is ≈1000 objects brighter than 17 mag. The overall completeness decreases to 62 per cent (1864 out of 2990 white dwarfs), given that most of these additional stars are in the range of $g = 16$–17.

3.4 Candidate selection

Having characterized the photometry of known white dwarfs, we can use our merged APG catalogue to identify new white dwarf candidates. In Fig. 8, we display three colour combinations and a reduced proper motion diagram for the known white dwarfs. We corrected *GALEX* photometry for non-linearity effects, using the results of Camarota & Holberg (2014). In the top-left panel of Fig. 8, DA white dwarfs are clearly distinct from main-sequence stars when they reach $T_{\rm eff} < 12\,000$ K (FUV − NUV > 1.3, NUV − g' > 0.5). In the top-right panel of Fig. 8, the (NUV − g', g' − r') combination of colours is a proxy for the more commonly used SDSS ($u - g, g - r$) diagram. The *GALEX* NUV band samples a spectral range that is further away from the Balmer jump, resulting in a less stretched distribution of colours. We note a fairly good agreement between observed colours and the white dwarf cooling tracks, with an amount of scatter that is mostly due to the larger uncertainties of the APASS r' magnitudes. It is worth noting the larger offset of some of the stars towards redder colours, which is a clear signature of the presence of late-type companions. The colour excess due to late-type companions becomes markedly evident when using 2MASS magnitudes, i.e. in the (NUV − g', NUV − H) panel of Fig. 8. Finally, the reduced proper motion diagram in the bottom-left corner of this figure confirms the bulk of the re-identified stars as nearby, fast moving objects.

To select white dwarf candidates, we applied an (NUV − g', g' − r') cut based on the colours of the re-identified stars (Fig. 8). This colour cut reduces the contamination from main-sequence stars that may share a similar colour space with white dwarfs of $T_{\rm eff} \lesssim 7000$ K. We then defined a selection criterion following the work of Gentile Fusillo et al. (2015) on SDSS, which establishes a probability for an object to be a white dwarf. This probability, $P_{\rm WD}$, is inferred from the colours and the reduced proper motion of known white dwarfs in the (H_g, g' − r') plane. Given the larger uncertainties of PPMXL proper motions with respect to those from SDSS, we only define objects with $\delta\mu/\mu \leq 0.3$ and $P_{\rm WD} > 0.75$ to be good white dwarf candidates. Below this value, we found that the APASS-PPMXL probabilities disagree by more than ± 25 per cent with those measured by Gentile Fusillo et al. (2015) for a sample of ≈300 stars in common.

We identified 8000 objects within our colour-cut, of which ≃1200 have $P_{\rm WD} > 0.75$. Given the strict $P_{\rm WD}$ requirement, not all the known white dwarf fall within this selection, mostly because PPMXL proper motion uncertainties weight down their probabilities. In this group of objects, we identified 392 that had not yet been spectroscopically confirmed as white dwarfs, 10 of which are GD stars. We observed 77 high priority objects, confirming 71 white dwarfs and 6 hot subdwarfs. Due to scheduling constraints, we also included in our target list objects that fall outside the colour-cut or with $P_{\rm WD} < 0.75$, achieving a lower rate of confirmed white dwarfs.

After our spectroscopic follow-up, we are left with 305 high-confidence white dwarf candidates with $P_{\rm WD} > 0.75$ and 33 GD

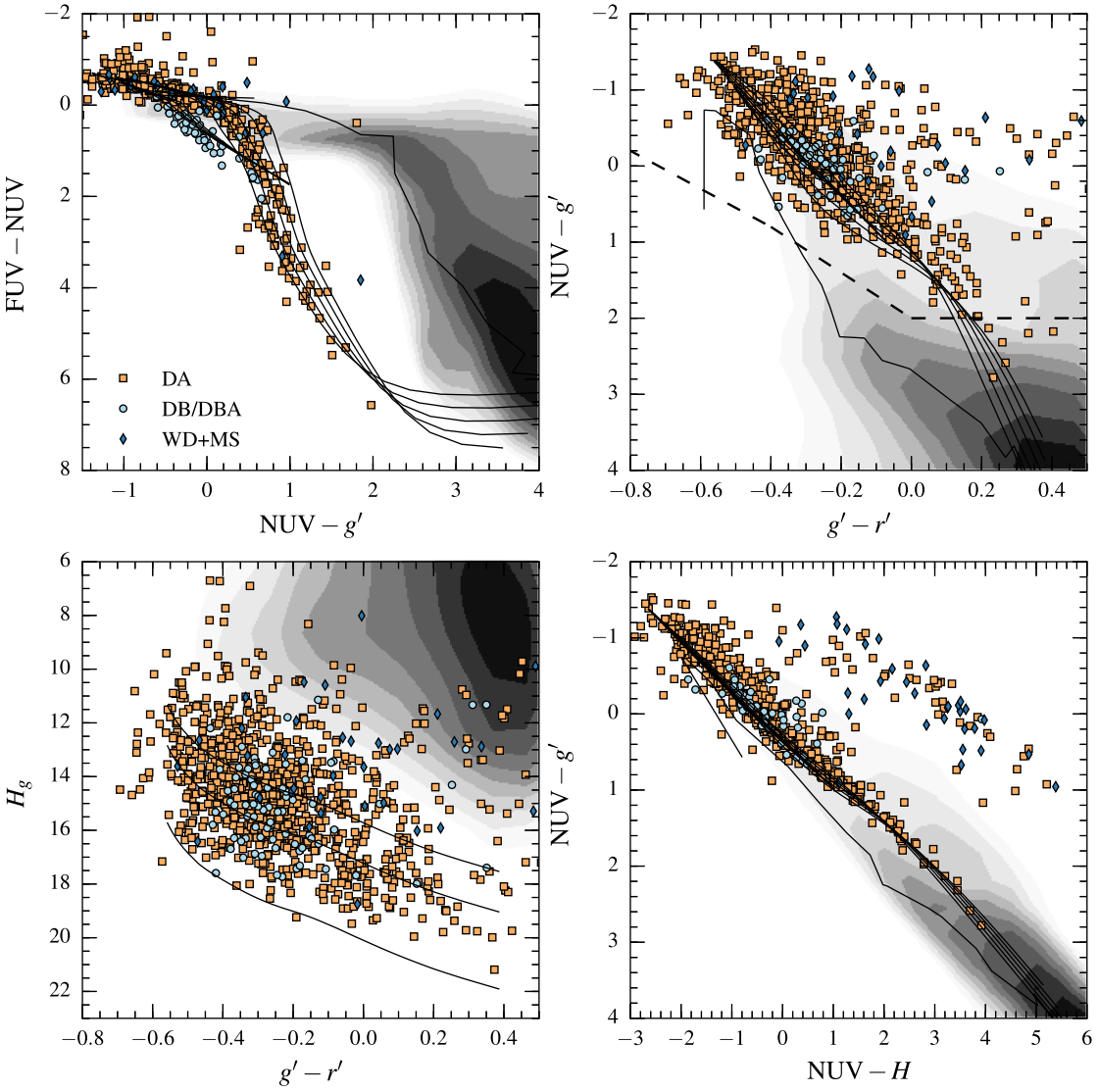

Figure 8. Colour–colour and reduced proper motion diagrams, obtained by combining *GALEX*, APASS and 2MASS photometry. The number of objects plotted in each panel depends on the availability of the data (refer to Table 3 and Fig. 6). The dark coloured contours in both panels represent the colour distribution of the field population, as inferred from our all-sky cross-match. Symbols used to distinguish distinct classes of white dwarfs are listed in the top-left panel. The dashed curves in the top-right panel delimit the colour space where most known white dwarfs are found. White dwarf cooling sequences ($\log g = 7.5$–9.5 in 0.5 dex steps) and main sequence are plotted for reference in the three colour–colour diagrams. The expected proper motion curves for $\log g = 8$ Galactic disc white dwarfs are plotted in the bottom-left diagram. Also refer to the caption of Fig. 3 for further details.

stars that do not have spectra or known spectral classification in the literature. In Fig. 9, we display the (NUV $- g', g' - r'$) colour–colour diagram of the candidate stars. In the lower panel of Fig. 9, the histogram bars represent the $P_{\rm WD}$ of all objects with $g' - r' \leq 0.5$ and NUV $- g' \leq 4$, i.e. about 1.5 million objects. We overlay step-histograms representing the $P_{\rm WD}$ of the known white dwarfs discussed in the previous sections, those for the 305 candidate white dwarfs, and those of white dwarfs and hot subdwarfs that we spectroscopically followed up.

The photometry and proper motions for the 305 white dwarf candidates are made available through VizieR in the format as listed in Table A1. The photometry for the 135 stars that we have followed up will also be hosted on VizieR, with the inclusion of an additional column, 'short name', which we use through the paper to refer to specific stars.

4 SPECTROSCOPIC FOLLOW-UP

We obtained low-resolution spectra for 135 stars covering the wavelength range from the Balmer jump to slightly beyond the Hα (3700–7500 Å). The observations were spread over 2.5 yr (2014 June/July, 2015 March/May and 2016 November/December), and the data were taken at three different telescopes: the 3.6-m New Technology Telescope (NTT) at the ESO La Silla observatory, the 2.5-m Isaac Newton Telescope (INT) at the Roque de Los Muchachos Observatory and the 1.82-m Copernico Telescope at the Ekar Asiago Observatory. Our targets were drawn from the APG list of candidates, the GD sample and some objects that have lower $P_{\rm WD}$. We note that some of the targets (8 white dwarfs and 10 subdwarfs; see next sections) were previously known in the literature but with poorly accurate coordinates, or that other research groups obtained classification during our follow-up operations.

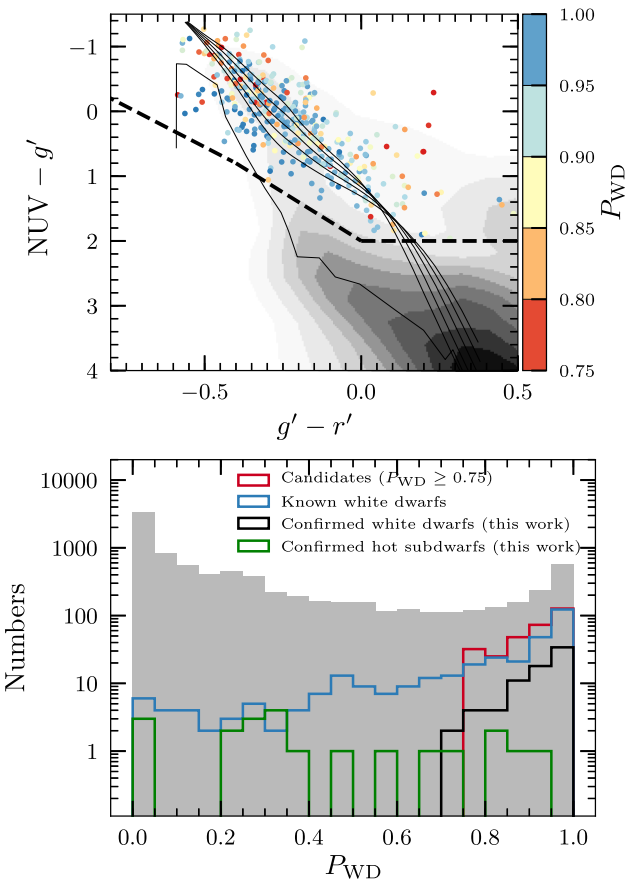

Figure 9. Selection of white dwarf candidates. *Top panel*: colour–colour diagram showing the colour-cut (dashed lines) applied to select white dwarf candidates. The side-bar codes the assigned probability of being white dwarf, $P_{\rm WD}$, based on the reduced proper motion information. *Bottom panel*: histogram distribution, on a logarithmic scale, of 1.5 million objects with $g' - r' \leq 0.5$ and NUV $- g' \leq 4$, which we bin in ranges of $P_{\rm WD}$. We overlay the histogram distribution of $P_{\rm WD}$ for known white dwarfs, candidate white dwarfs, and the white dwarfs and hot subdwarfs that we confirmed spectroscopically.

Table 4. Summary of instruments and number of spectra for the follow-up discussed in this paper.

Telescope	Set-up	Δλ (Å)	Slit (arcsec)	Date	*N*
NTT	EFOSC2/# 11	9.5	0.70	2014/06/13–15	48
		6.5–9.5	0.70	2014/07/11–13	34
INT	IDS/R400V	3.5	1	2015/03/03–06	46
		3.5	1.0	2015/05/12–18	38
Copernico	AFOSC/VPH7	13	1.25	2016/11/05	2
		13	1.25	2016/12/26–30	7

At the NTT, we used the ESO Faint Object Spectrograph and Camera 2 (EFOSC2; Buzzoni et al. 1984) with the # 11 grism, a slit of 0.7 arcsec and binning 2 × 1 and 2 × 2, obtaining a resolution of 6.5–9.5 Å. The set-up adopted at the INT produced a 3.5 Å resolution, mounting the Intermediate Dispersion Spectrograph (IDS) with the grating *R*400*V* a slit of 1 arcsec and the blue-sensitive EEV10 CCD. For the Copernico set-up, we mounted the Asiago Faint Object Spectrograph and Camera (AFOSC) with the volume phase holographic grating, VPH7 (Zanutta et al. 2014), and a slit of 1.25 arcsec, which deliver a resolution of 13 Å with a 2 × 2 pixels binning. The log of the observations is summarized in Table 4.

Table 5. Summary of spectral classification.

Type	Number
White dwarfs (total)	82
DA	60
DA+MS	9
DAH	1
DAB	1
DB/DBA	4
DC	7
Hot subdwarfs/BHB	25
Other stars	28

The observations were done under different sky illumination (grey/bright at the NTT, dark/bright at the INT, dark/grey at the Copernico), with the seeing typically <2.5 arcsec, variable weather conditions often with thin clouds and during non-photometric nights (especially during the second run at NTT, the second run at INT when calima affecting the sky transparency occurred and the November runs at Asiago that were affected by high humidity). We took two to four exposures per target, with exposure times in the range of 300–1800 s. On several occasions, we obtained multiple spectra of the same object across different runs to improve the total signal-to-noise ratio.

We took standard calibration frames (bias, dome flats) during each run, and arc lamps before and after the targets at the NTT and INT. We obtained a few arc lamps at beginning of the Asiago run (Ne and Hg+Cd separately, later combined during the data reduction), which were sufficient for an approximate wavelength calibration of the low-resolution spectra. We also observed two to three spectrophotometric standards per night with a 5-arcsec slit and we placed the slit at the parallactic angle for all the science and standard stars, in order to minimize flux-loss and to obtain a relative flux-calibration of the spectra, shown to be in good agreement with APASS photometry for most of the confirmed white dwarfs. A few exceptions are the visually resolved WD+MS pairs, where we rotated the slit to include both the white dwarf and the late-type companion.

We used standard reduction routines to subtract the bias, to apply the flat-field correction and wavelength calibration, to optimally extract the 1D spectrum, and for the flux calibration. Specifically, we used the STARLINK suite of programs including PAMELA[9] (Marsh 1989) and MOLLY.[10]

4.1 Spectral classification

From a visual inspection of the multiple observations, we selected the best spectra for each star that we used for a quantitative classification. These spectra have a typical signal-to-noise ratio larger than 20. We confirmed 82 white dwarfs (8 of which were previously known) and 25 hot subdwarfs/blue horizontal branch (BHB) stars (10 of which were previously known). We classify the remaining 28 objects as A/F/G dwarfs, some of which have apparently large proper motions and colours that overlap with those of cool white dwarfs (see Fig. 18).

The breakdown of the sample by subtype is summarized in Table 5. We identify 71 hydrogen atmosphere white dwarfs; in

[9] http://starlink. eao.hawaii.edu/starlink
[10] http://www.warwick.ac.uk/go/trmarsh/software/

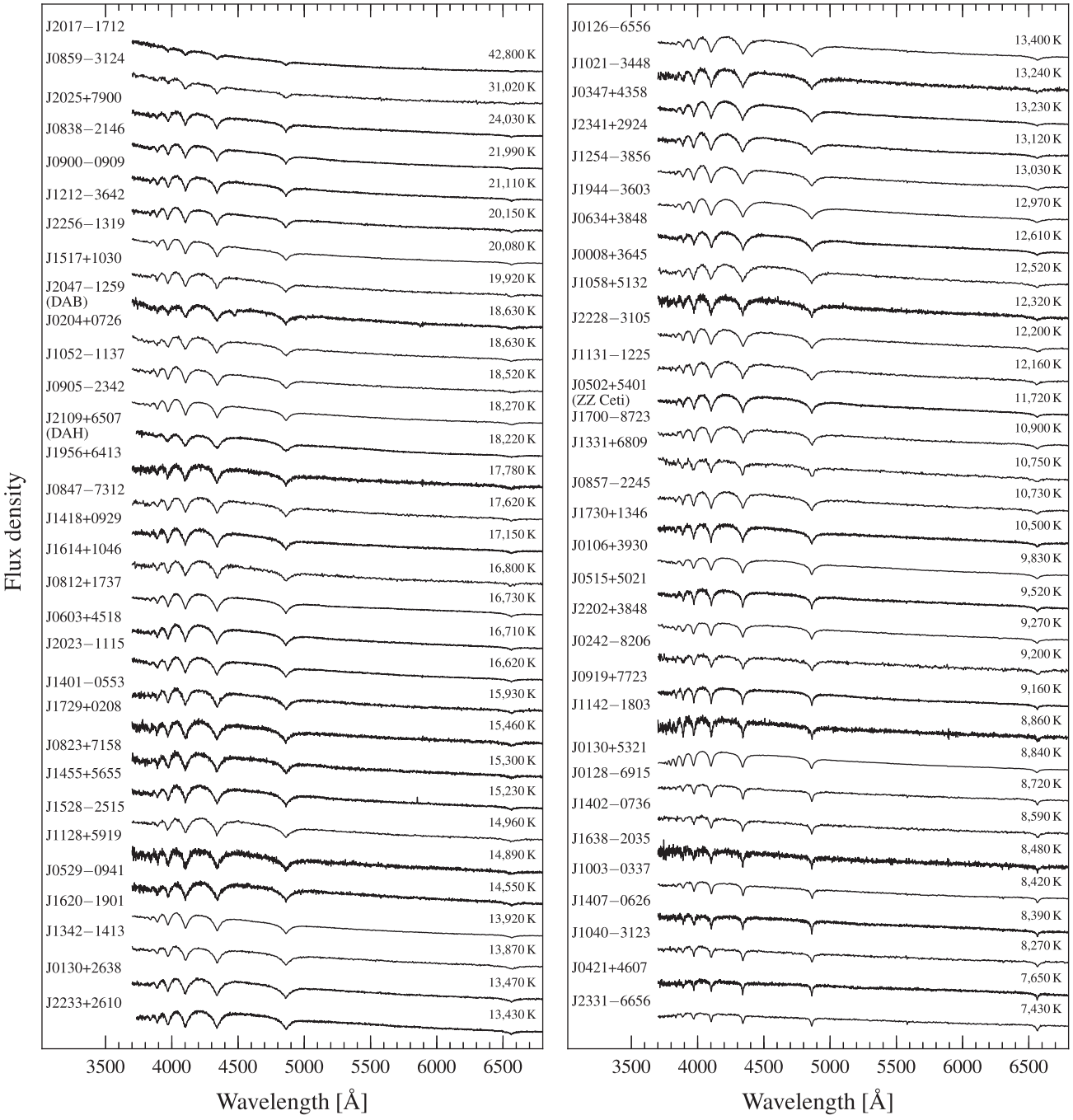

Figure 10. Spectra of the single hydrogen-atmosphere (DA) white dwarfs, sorted by temperature. Wherever, relevant, subtypes are included between brackets.

Fig. 10, we show 60 single objects (DA), one magnetic white dwarf with Zeeman splitting of the Balmer lines (DAH) and another that presents also helium lines (DAB). We classify nine white dwarfs as binaries with a late-type companion (DA+MS), either on the basis of the near- and mid-infrared excess detected by 2MASS and *WISE* or from spectroscopic evidence (Fig. 11). Three of these systems were visually resolved at the NTT, and thus we took spectra at non-parallactic angles to include both stars in the slit. One star, J1022−3226, displays also a weak Hα emission line that could be produced from a chromospherically active companion. Finally, we found four DBA white dwarfs, six objects that do not present any clearly detectable spectral features (DC) at the quality of our data (with the exception of J1010−2327, which has broad features in the blue part of the spectrum that may be either due to the presence of carbon in the atmosphere or to a strong magnetic field); their spectra are shown in Fig. 12.

We will not discuss the spectral classification of the hot subdwarfs and BHB stars in detail here. We roughly estimated their $T_{\rm eff}$ via a photometric fit to the NUV$BVg'r'$ photometry, using DA models with $\log g = 6$. We note that some of the stars have composite spectral energy distributions (SEDs), which indicate the presence of a late-type companion. We display the

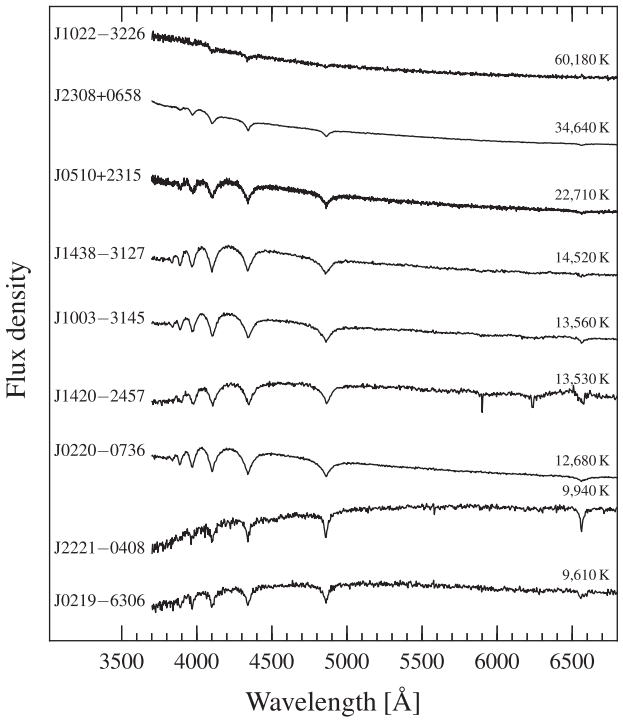

Figure 11. DA+MS binaries sorted by temperature.

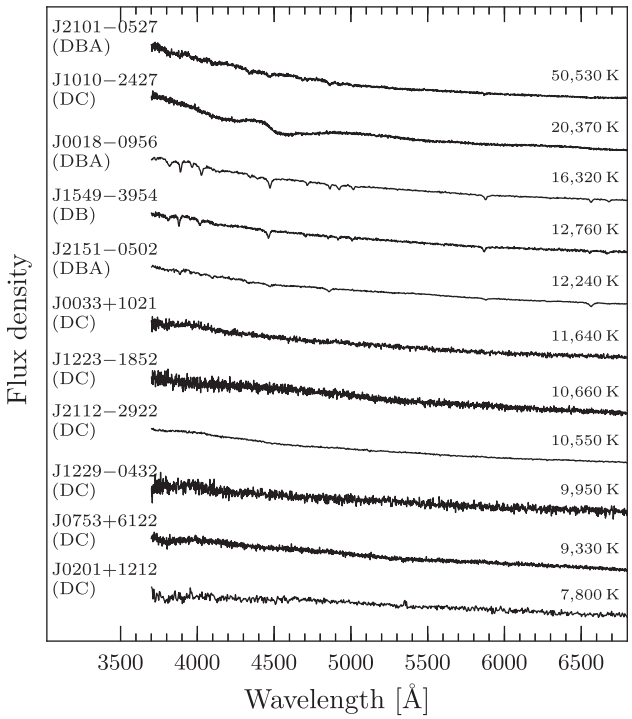

Figure 12. DBA and DC white dwarfs.

spectra of these 25 stars in Fig. 13, noting they span a range of temperatures between 11 000 and 24 000 K. For the previously known stars, we advise the reader to refer to the existing literature.

4.2 Atmospheric parameters of the spectroscopically confirmed white dwarfs

For the determination of temperature and surface gravity ($T_{\rm eff}$, $\log g$) of the white dwarfs we used the software FITSB2, which estimates a best fit via χ^2 minimization using a downhill simplex algorithm (Napiwotzki et al. 2004). The $T_{\rm eff}$ and $\log g$ uncertainties were estimated via a bootstrap method. We used the Koester (2010) model atmospheres, which adopt a ML2/$\alpha = 0.8$ mixing-length prescription for convective atmospheres and the Stark broadening profiles of hydrogen lines computed by Tremblay & Bergeron (2009).

For the 60 DA single white dwarfs, we fitted six Balmer lines (Hα–H8), while we excluded the Hα and Hβ from the fit for the nine DA+MS pairs when the spectral profiles were altered by the presence of the companion star. A few examples of the best-fitting results are shown in Fig. 14, illustrating the quality of both the data and the fits. We also display in Fig. 15 an example of how the signal-to-noise ratio in the proximity of Balmer lines and spectral resolution are the relevant factors in assessing the surface gravity of selected objects, chosen at $T_{\rm eff} \approx 10\,000$ K and $T_{\rm eff} \approx 20\,000$ K. To estimate $T_{\rm eff}$ of non-DA white dwarfs, we used a photometric technique fitting the available ultraviolet/optical data and keeping $\log g = 8$ fixed.

From the Copernico/AFOSC observations, we identified J0130+5321 (GD 278) for which we had to arbitrarily fix $\log g = 6$ to obtain a satisfying fit of the spectrum and photometry. Its spectrum was acquired in good weather conditions, and presents only hydrogen lines at the resolution of the AFOSC set-up.

The atmospheric parameters of the 60 single DA white dwarfs and nine DA+MS white dwarfs are listed in Table B1. The eight stars that were previously known are J0347+4358 J0502+5401, J0812+1737, J1455+5655 and J2233+2610 (Limoges et al. 2013, 2015), J0847−7312 (Gianninas et al. 2010), J1003−0337 (GD 110; Kepler et al. 1995) and J1128+5919 (Girven et al. 2011). Our results for $T_{\rm eff}$ and $\log g$ agree within 2σ–3σ with those reported in the literature.

Among the hydrogen-dominated atmospheres, there are two peculiar objects. One is a magnetic white dwarf (DAH), J2109+6507, for which we kept $\log g = 8$ fixed and derived its $T_{\rm eff}$ through a fit of the photometric data. The second object is a DAB white dwarf, J2047−1259. We obtained two spectra, the first taken at the NTT on 2014 June and the second at the INT on 2015 May, which do not show sensible differences in the relative position and appearance of spectral features. We initially estimated a $T_{\rm eff} = 17\,000 \pm 740$ K and $\log g = 9.0 \pm 0.1$, using only the Balmer lines. We then attempted a fit with a grid of DAB model spectra, which sample different [H/He] compositions. In Fig. 16, we show the improved agreement with a synthetic spectrum of $T_{\rm eff} = 18\,630 \pm 360$ K, $\log g = 8.37 \pm 0.06$, and [H/He] $= -1$. The quality of our radial velocity information does not exclude the possibility that this system could be a close binary pair.

5 PHYSICAL PARAMETERS

We estimated masses and ages for the DA white dwarfs, the DAB white dwarf and the DA+MS white dwarfs. We interpolated the physical parameters from the Montréal cooling tracks, using the spectroscopic estimates of $T_{\rm eff}$ and $\log g$. For $T_{\rm eff} < 30\,000$ K, we used the carbon–oxygen core cooling models with thick hydrogen layers, which are described by Fontaine et al. (2001). For hotter stars, we used the carbon-core cooling sequence of Wood (1995). We applied the Tremblay et al. (2013) 3D corrections to the measured

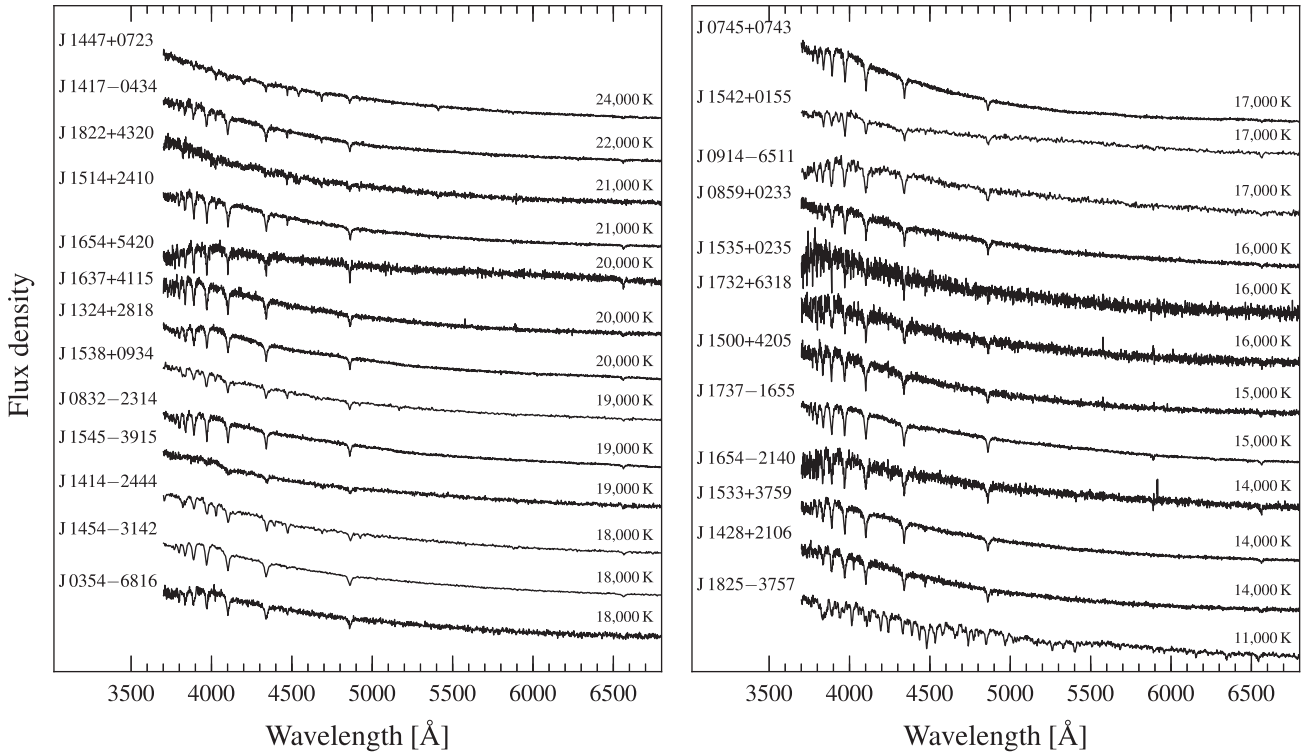

Figure 13. Hot subdwarfs and BHB stars sorted by temperature.

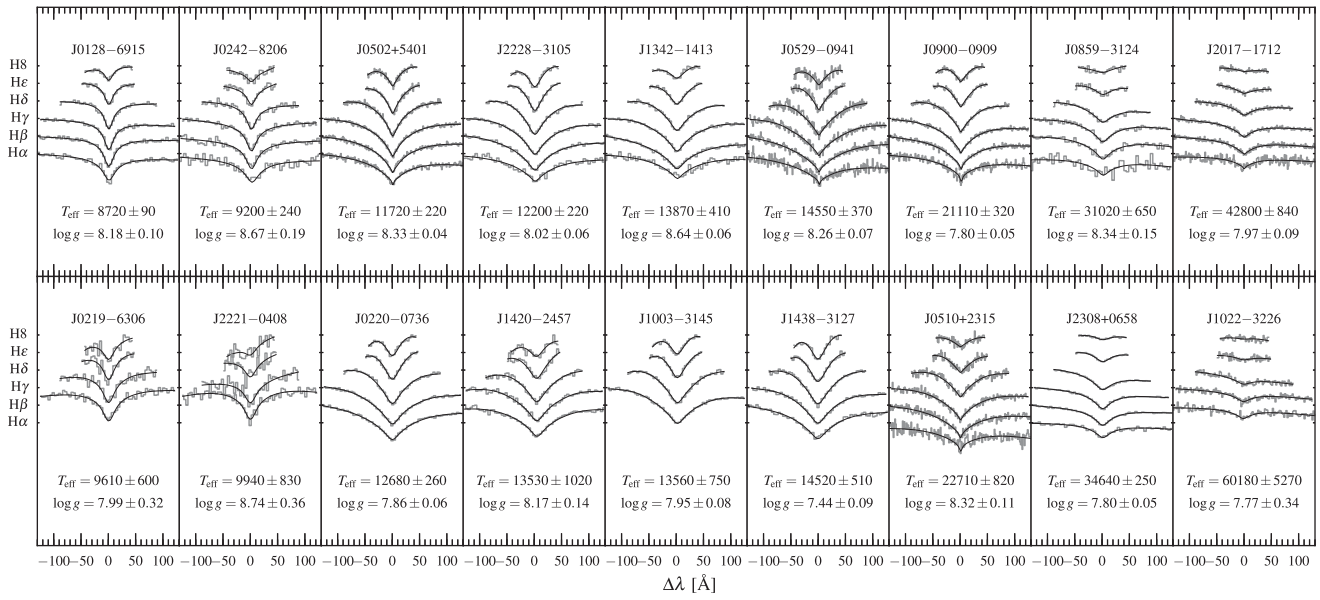

Figure 14. Best fits of the Balmer lines for selected single DA white dwarfs (top row) and those in DA+MS pairs (bottom row). Synthetic spectra (black) are overlaid on to observed spectra (grey).

atmospheric parameters of cool DA white dwarfs ($T_{\rm eff} < 15\,000$ K), which account for the inaccurate treatment of convection in 1D model atmospheres. The physical parameters and the 3D corrections are given in Table B1. The distribution of hydrogen-dominated white dwarfs in the ($T_{\rm eff}$, $\log g$) plane is displayed in Fig. 17, where most stars are found to have $\log g = 8.00 \pm 0.25$.

Seven stars have atmospheric parameters that are compatible with the instability strip of DA white dwarfs (Gianninas et al. 2015; Tremblay et al. 2015). One is the already known ZZ Ceti star, J0502+540 (Green et al. 2015; Limoges et al. 2015), for which we give more details in Section 6.4. The other six stars are candidate pulsators (cZZ in Table B1).

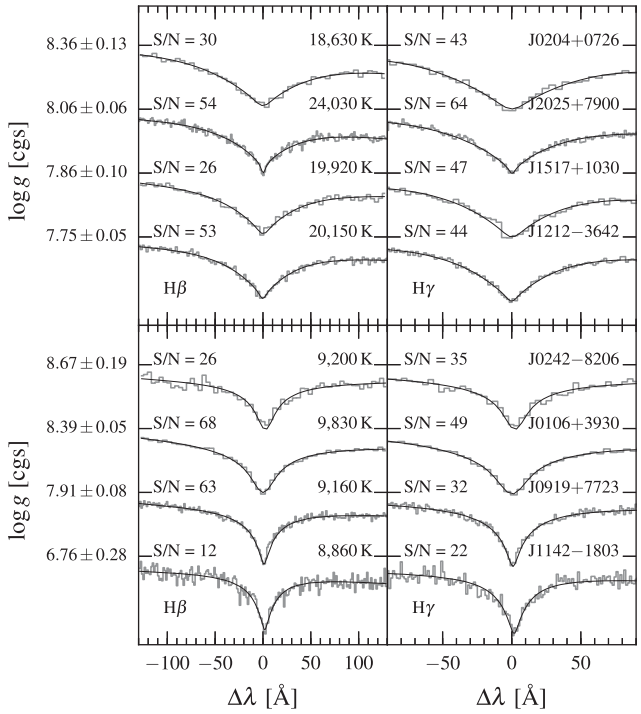

Figure 15. Best fits of H β and H γ lines for selected objects with $T_{\rm eff} \approx$ 20 000 K (top row) and ≈10 000 K (bottom row). Objects are plotted in order of decreasing $\log g$. Synthetic spectra (black) are overlaid on to observed spectral lines (grey).

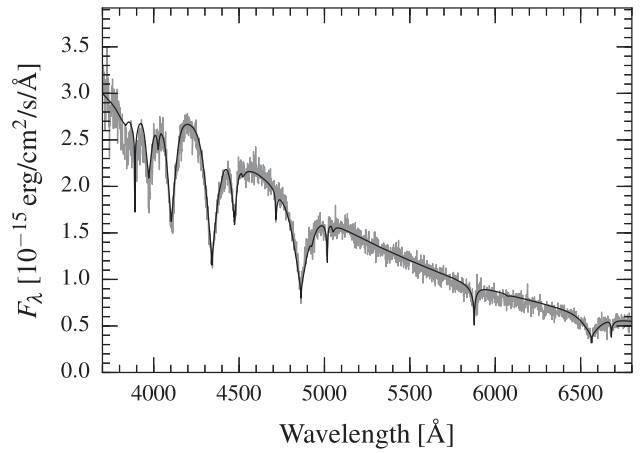

Figure 16. Observed spectrum (grey) of the DAB white dwarf, J2047−1259, and the best-fitting model spectrum (black) with $T_{\rm eff} = 18\,630 \pm 360$, $\log g = 8.37 \pm 0.6$ and [H/He] = −1.

Two low surface gravity stars, J0130+5321 (GD 278) and J1142−1803, could potentially be extremely low mass white dwarfs. J0130+5321 would have a mass of ≈0.16 $M_\odot$ (cf. fig. 3 in Brown et al. 2010). J1142−1803 was previously classified as a subdwarf (sdB) by Kilkenny et al. (1997). It has narrow spectral lines as expected for a cool white dwarf ($T_{\rm eff} \approx$ 9000 K). This star has an NUV − g' colour that locates it between the white dwarf cooling tracks and the main sequence in the top-left panel of Fig. 18, in agreement with the low surface gravity estimate ($\log g = 6.76 \pm 0.28$), corresponding to ≈0.21 $M_\odot$. Given that we used low-resolution gratings, we cannot rule out that at least GD 278 is a metal-poor halo star (Brown, Kilic & Gianninas 2017). Nevertheless, we note that both stars have relatively large proper motions that are compatible with those of white dwarfs.

6 DISCUSSION

6.1 Interstellar reddening

The sample of white dwarfs discussed here is made up of relatively bright, but intrinsically low-luminosity objects; thus, these are mostly nearby and suffer very little reddening. In Fig. 18, we display a selection of colour–colour and reduced proper motion diagrams for the observed stars, which offer a visual comparison with the same plots for the known white dwarfs from the literature (Fig. 8). The confirmed white dwarfs and subdwarfs are all located within the dashed lines that we have chosen as colour cut for the identification of white dwarf candidates in Section 3.4. The only exception is the DC white dwarf, J0201+1212 (GD 21). The contaminants, also shown in this figure, are mostly outside the dashed lines and share the colour space of cool ($T_{\rm eff} < 7000$ K) white dwarfs. Finally, we stress that the presence of cool companions to white dwarfs and hot subdwarfs is clearly evident in rightmost panels of Fig. 18, where these objects depart from their typical single-star colours.

To confirm stars we observed are affected only by a small amount of interstellar reddening, we estimated the colour excess in four different colours in Fig. 19. The leftmost panel of this figure displays the colour excess in the UV bands. Although we attempted an empirical correction to reduce non-linearity effects of *GALEX* photometry (Camarota & Holberg 2014), a few hot stars (FUV−NUV < 0.2 mag) still have negative UV excess. This could be due to a wrong fit of the Balmer lines, leading us to overestimate $T_{\rm eff}$. However, in $B - V$ and $g' - r'$, most stars are consistent with $E(B - V) \leq 0.1$. Finally, the NUV−H colour in Fig. 19 clearly reveals the colour excess of the DA+MS systems due to the strong H-band contribution of their companions. We note that a few other stars follow the same trend as the DA+MS stars, although with smaller colour excess. However, given that their 2MASS H and K_s are only upper limits, we exclude the presence of unseen companions.

6.2 Comparison with *Gaia*

Gaia data release 1 (DR1; Gaia Collaboration 2016b) photometry became public last year. Due to known issues with the chromatic correction in the astrometry of *Gaia*, not all the identified sources have been released (1 per cent of the total number of detected sources; van Leeuwen et al. 2017). This problem has affected especially blue objects such as white dwarfs, including the *Tycho/Hipparcos* objects that could already have parallaxes (Tremblay et al. 2017)

We searched the *Gaia* data base within 1 arcsec from the APASS coordinates of the 135 stars for which we have follow-up spectroscopy. We could find G_p photometry for only 61 of them, including 42 white dwarfs or hot subdwarfs. In Fig. 20, we display the comparison between *Gaia* and APASS magnitudes. The underlying distribution represents the photometry for the GD sample, while we overlay on top the stars we have followed up spectroscopically. About 70 per cent of the GD sample was retrieved successfully.

We find a that the good correlation in the range of $g' - r'$ colours covered by our sample. There are just a few outliers, and the correlations appear to depart from linearity for $g' - r' < -0.3$; however, we identified fewer objects in this magnitude range. The most discrepant object is J1212−3642 (not shown in Fig. 20), whose APASS

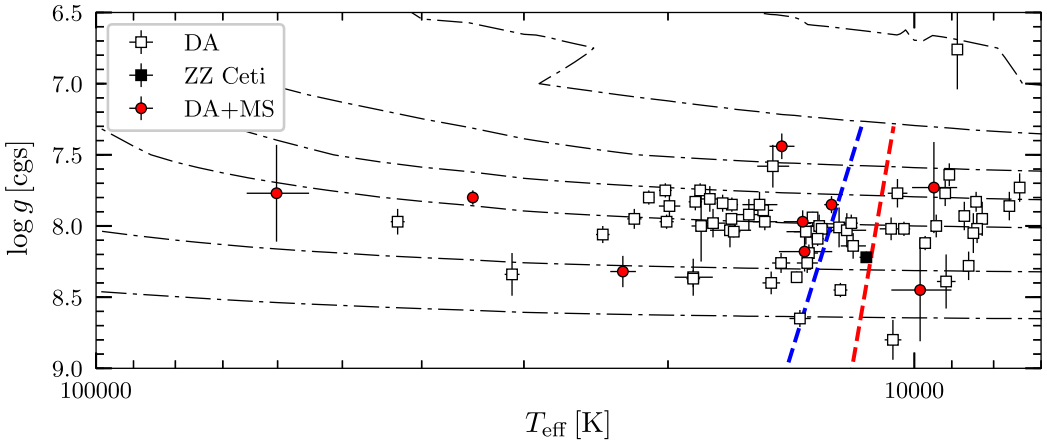

Figure 17. Atmospheric parameters of DA white dwarfs. The Fontaine, Brassard & Bergeron (2001) cooling tracks are overplotted as dash–dotted curves for 0.2, 0.3, 0.4, 0.5, 0.6, 0.8 and 1.0 $M_{\odot}$ from top to bottom, respectively. The empirical red and blue $T_{\rm eff}$ limits of the instability strip are shown (dashed lines; Gianninas et al. 2015). We mark in black one confirmed ZZ Ceti star, J0502+5401.

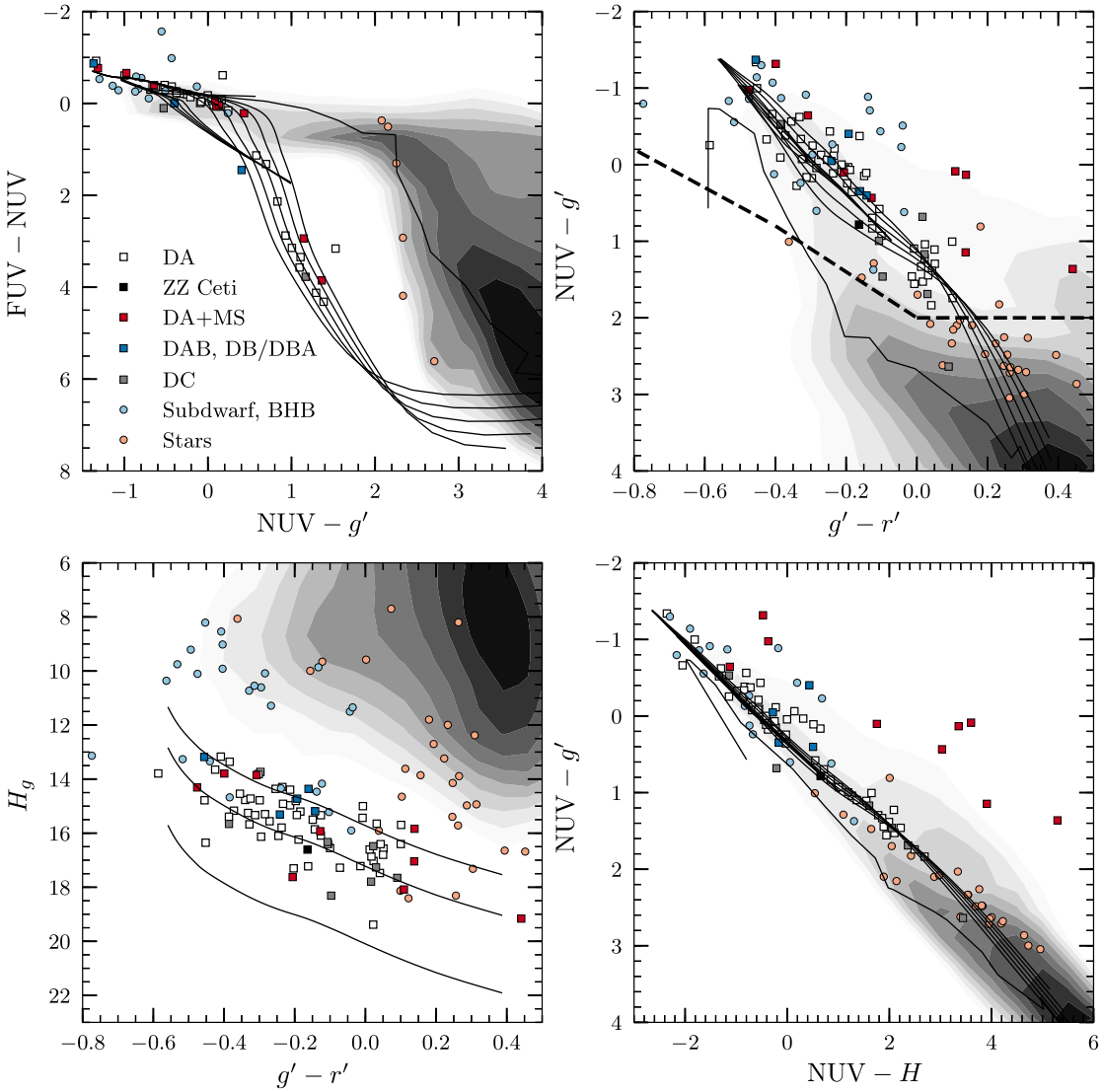

Figure 18. Colour–colour and reduced proper motion diagrams of the 135 stars we have followed up. Symbols are clarified in the legend. For a description of synthetic tracks refer to Fig. 8.

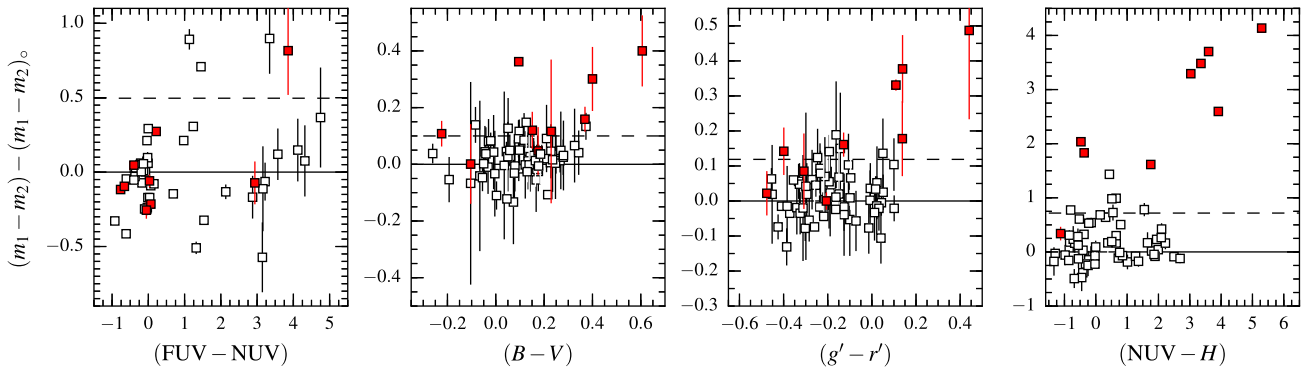

Figure 19. Assessment of the colour excess for the white dwarf sample. Each panel represents a set of colours, which combine from left to right *GALEX*, APASS and *GALEX*-2MASS bands. On the *y*-axis is the colour excess, i.e. the observed minus the intrinsic colours. The dashed line marks the $E(B-V) = 0.1$ colour excess in each panel. DA white dwarfs are plotted as white squares, red symbols are used for the DA+MS pairs, which appear with strong NUV − *H* excesses. Generally, this spectroscopic follow-up sample has minimal interstellar reddening.

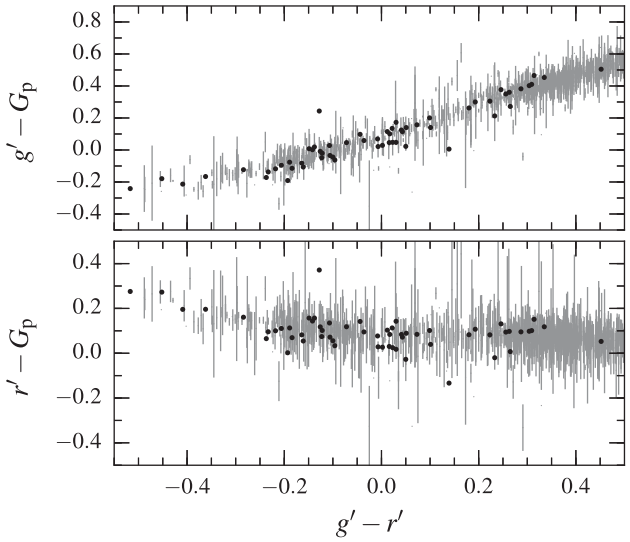

Figure 20. Comparison between *Gaia* G_p, APASS g' and r' magnitudes, plotted against $g' - r'$ colours.

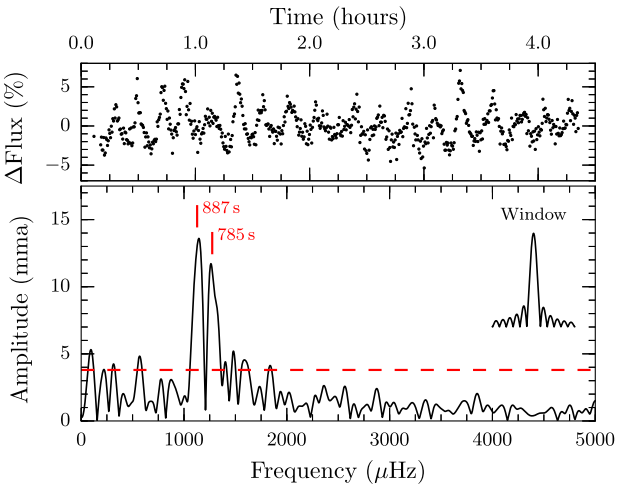

Figure 21. Confirmation of pulsations for J0502+540. The 4.5-h light curve taken at the Warwick 1-m Telescope is shown in the top panel; the discrete Fourier transform is displayed in the bottom panel. The two main peaks are labelled, and the 3σ threshold is displayed as a red line. In the right corner is the window function that illustrates the frequency resolution of the discrete Fourier transform.

g' and r' photometry is ≈1 mag fainter with respect to *Gaia* G_p. *Gaia* DR1 contains only one source at 0.6 arcsec from the coordinates of J1212−3642. It does not present detectable infrared excess or spectral peculiarities. With this information in hand, we suggest that APASS photometry could be systematically off. Other two spectroscopic objects that differ by 0.2–0.3 mag from the one-to-one correlation, J1003−3145 and J1438−3127, are DA+MS binaries for which the presence of a companion can be the source of photometric variability.

6.3 White dwarf distances

We estimated spectroscopic distances by considering no extinction, but we assumed an average scatter of $E(B-V) = 0.03$ that corresponds to 0.1 mag of extinction in the g' band. We estimated the intrinsic g'-band magnitudes by convolving the filter profile to appropriately scaled (Koester 2010) synthetic spectra. We propagated the $T_{\rm eff}$ and $\log g$ uncertainties in order to assess the scatter in synthetic magnitudes. We found that about 12 DA white dwarfs have spectroscopic parallaxes placing them within 40 pc from the Sun. Only J0812+1737 was previously known to be at less than 40 pc from the Sun (Limoges et al. 2013). Of the other 11 stars, 6 are in the Northern hemisphere and 5 in the south. The nearest white dwarf we identify is J1407−0626, for which we estimate a distance of 25 pc. This is a cool white dwarf ($T_{\rm eff} = 8400$ K), which has likely escaped previous searches due to its modest proper motion (≈0.1 arcsec yr^{-1}). Next year, the ESA *Gaia* mission will deliver accurate parallaxes for this object, confirming or refuting its membership to the local sample within 25 pc from the Sun.

The remaining DA white dwarfs are all within 100 pc from the Sun. The most distant white dwarf in the spectroscopic follow-up sample is in the hot DA+MS system, J1022−3226, at 288 pc.

6.4 ZZ Ceti stars

Fig. 17 identifies seven white dwarfs that fall within the instability strip of hydrogen atmospheres. One of the stars, J0502+540, was previously classified as ZZ Ceti by Limoges et al. (2015) and its pulsations confirmed by Green et al. (2015). We re-observed this star on 2016 January 6 at the Warwick 1-m Telescope in La Palma for ≈4.5 h with a 20-s cadence. In Fig. 21, we display the Fourier

Table 6. Physical parameters of the low-mass companions.

Name	$T_{\rm eff}$ (K)	Age (Gyr)	Mass ($M_\odot$)
J0219−6306 B[a]	2900 ± 170	2.05	0.09
J0220−0736 B	2300 ± 620	11.70	0.08
J0510+2315 B	2000 ± 380	0.40	0.05
J1003−3145 B	3000 ± 200	11.55	0.08
J1022−3226 B	2800 ± 1050	1.24	0.08
J1420−2457 B[a]	3000 ± 360	3.37	0.10
J1438−3127 B[b]	3300 ± 140	>2.30	
J2221−0408 B[a]	3200 ± 870	1.83	0.15
J2308+0658 B	4000 ± 480	1.80	0.7

Notes. [a]Not observed at parallactic angle. Resolved binary.
[b]Suggested post-common envelope binary.

transform of the light curve, where we identify two main periods in agreement with Green et al. (2015).

Among our sample, J2233+2610 was also observed by Green et al. (2015) and found not to be variable to above 0.07 per cent. This star is about 1000 K hotter than the empirical instability strip; thus, it is not expected to vary. The remaining candidates will be excellent targets for *TESS*, which will acquire detailed light curves enabling an unprecedented level of characterization for these and other ZZ Ceti stars. Furthermore, we stress that the brightest stars in our sample ($g < 16$) are ideal targets for ground-based observations, e.g. with Evryscope (Law et al. 2015) or NGTS (West et al. 2016) which currently provide detailed time-domain photometry with a large coverage of the Southern hemisphere.

6.5 Late-type companions

We identified nine white dwarfs in our sample that display redder colours than isolated objects (Fig. 19), which suggest the presence of late-type companion stars. We confirmed six of them based on spectroscopic evidence (e.g. composite spectra or the weak Hα emission seen in the spectrum of J1022−3226; Fig. 11). For three of these stars, labelled in Table 6, we could visually resolve the companions when we acquired their spectra. Three further systems are proposed to have companions that are too cool with respect to the white dwarf to reveal their presence in optical spectra (J0520+2315, J0220−0736 and J2308+0658), but displaying infrared excess already in the 2MASS *J* band.

We derived the $T_{\rm eff}$ of companion stars via fits to the composite SEDs, including *GALEX*, APASS, 2MASS and *WISE* *W*1/*W*2 photometry. We kept the atmospheric parameters of the white dwarfs fixed to those determined from the spectroscopic analysis (Table B1) and we built a grid of spectra for low-mass stars and substellar objects, taken from the latest version of the BT-Settl models (Allard et al. 2012). We fixed the models' metallicity to solar and $\log g = 5$. We derived the intrinsic magnitudes of white dwarfs and main-sequence stars by convolving the filter profiles with the appropriate models from the Koester (2010) library of synthetic spectra and the BT-Settl grid, respectively. Finally, we estimated the best fits through a χ^2 minimization of the available photometry with three free parameters, i.e. an absolute scaling factor, the relative flux of white dwarf and companion, and the atmospheric temperature of the secondary. The results of our fits are displayed in Fig. 22.

We also estimated the companion masses, under the assumption they are dwarf stars. Thus, we first considered a semi-empirical initial-to-final mass relation (Catalán et al. 2008), from which we inferred the white dwarf progenitor mass. We then estimated the total age of the system, by approximating the stellar lifetime with a simple

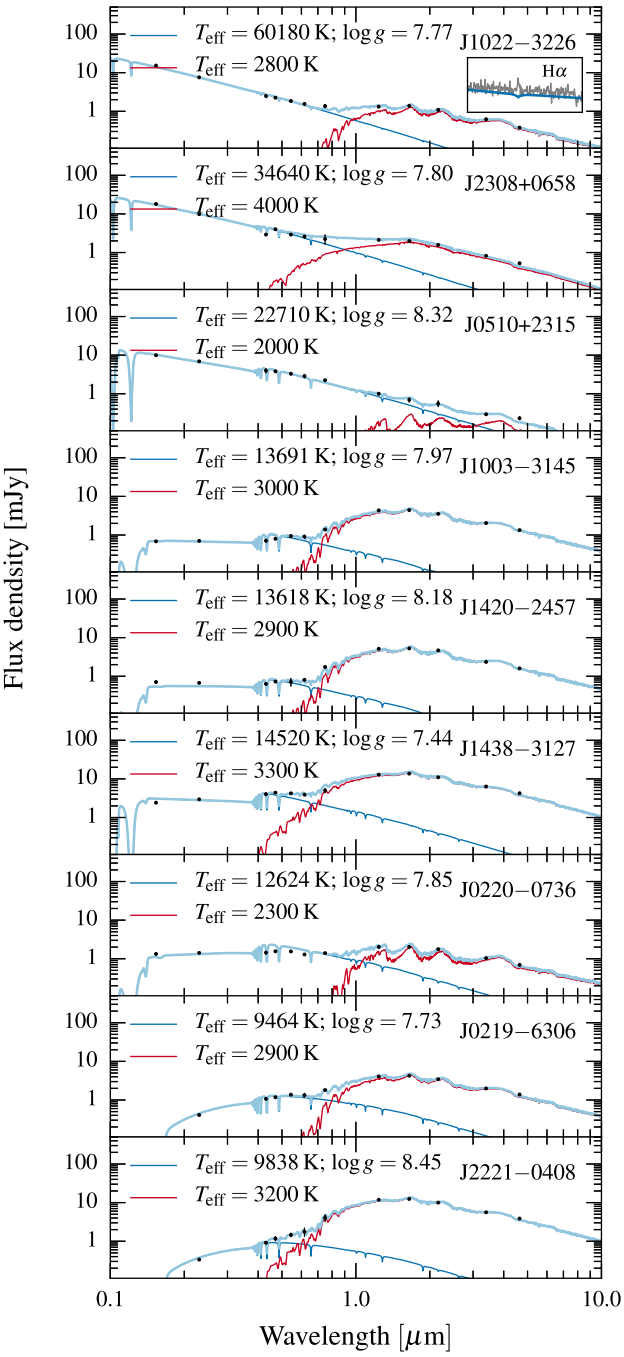

Figure 22. Photometric fits of the DA+MS binaries, sorted by descending white dwarf temperature (from top to bottom). We display the white dwarf spectra (in blue), the low-mass companions spectra (in red), and the combined spectra (in cyan). We display all the photometric bands available as black dots. In the top panel, we also plot a cut-out of the Hα region for J 1022−3226, for which we detect a weak emission.

analytical expression (e.g. Age $= 10 \times M_{\rm prog}^{-2.5}$ Gyr; Wood 1992). Finally, we determined the companion mass via interpolation of $T_{\rm eff}$ and age on the Baraffe et al. (1998, 2003) tracks for low-mass and substellar mass objects. In Table 6, we list the relevant physical properties of the companions ($T_{\rm eff}$, age and mass).

We found that most of the proposed companions have masses in the range of 0.1 $M_\odot$, i.e. corresponding to late-M spectral types. Spectroscopic follow-up aiming at a better characterization of these

companions is necessary, especially for the least massive of them, J0510+2315 B, that we only identify through its infrared excess. For this object, we infer a mass of 0.05 $M_\odot$, compatible with a brown dwarf. Although the first brown dwarf candidate to be discovered, GD 165 B, is a companion to a known white dwarf (Becklin & Zuckerman 1988), substellar white dwarf companions are rare, with an occurrence rate of at most a few per cent, estimated from high contrast imaging techniques (Farihi et al. 2005; Hogan, Burleigh & Clarke 2009), transit surveys (Faedi et al. 2011) and searches for infrared excess (Girven et al. 2011; Steele et al. 2011).

Another system worth mentioning is J1438−3127, for which we estimated a white dwarf mass of $0.36 \pm 0.04\,M_\odot$. A white dwarf of such a low mass could not have been formed in isolation within a Hubble time, implying it could be the product of binary interaction. Rebassa-Mansergas et al. (2011) showed that low-mass white dwarfs are more frequent in short-period (post-common envelope) binaries than in the field or in wide binary systems, bringing observational evidence in support to binary interactions during the common envelope phase. Such low-mass white dwarfs are suggested to have gone through the common envelope phase while on the first giant branch, implying that their progenitors had an initial mass of $\lesssim 1.8\,M_\odot$ (Zorotovic & Schreiber 2013) and consequently a lifetime of $\gtrsim 2.3$ Gyr. Given that the evolution of such systems is complicated by the common envelope phase, we do not derive a companion mass as done for the other binaries.

7 CONCLUSION

We have produced a catalogue of bright white dwarf targets for the upcoming NASA *TESS* mission as well as long-baseline photometric surveys such as Evryscope and NGTS. The target list was compiled by cross-matching APASS, PPMXL and *GALEX*. The catalogue includes proper motions and multiband photometry for 1864 known white dwarfs brighter than 17 mag. Having validated our cross-match against the Lowell Observatory proper motion survey (Giclas et al. 1980) and catalogues of spectroscopically confirmed white dwarfs, we identified 428 high confidence white dwarf candidates (including 46 GD stars). We presented follow-up spectroscopy for 82 white dwarfs and 25 hot subdwarfs/BHB stars (8 white dwarfs and 10 subdwarfs in the sample were previously known). Among the confirmed white dwarfs, we have identified a few interesting objects, such as a DAB white dwarf, six bright ZZ Ceti star candidates, nine WD+MS binaries, and one white dwarf at 25 pc from the Sun. This leaves 305 high-confidence white dwarf candidates and 33 GD stars requiring follow-up spectroscopy to ascertain their nature.

The uninterrupted light curves that *TESS* will obtain for the proposed stars, will provide unprecedented insight on their variability (ZZ Ceti stars), binary eclipses, as well as important statistical information on transits from exoplanets or debris around white dwarfs. The 30-min full-frame exposures of the *TESS* mission will increase the chances of finding serendipitous transits, by also monitoring stars that are not included in the short-cadence list of targets.

We publish the collection of photometric data for all the previously know white dwarfs that we re-identified in our analysis, which will become particularly useful with *Gaia* DR2 in spring 2018. Statistical analysis of spectroscopy, photometry and parallaxes can eventually be used to obtain a very accurate estimate of cooling ages (e.g. O'Malley, von Hippel & van Dyk 2013; Si et al. 2017) for this sample of known white dwarfs.

ACKNOWLEDGEMENTS

This research was made possible through the use of the AAVSO Photometric All-Sky Survey (APASS), funded by the Robert Martin Ayers Sciences Fund.

Some of the data presented in this paper were obtained from the Mikulski Archive for Space Telescopes (MAST). STScI is operated by the Association of Universities for Research in Astronomy, Inc., under NASA contract NAS5-26555. Support for MAST for non-*HST* data is provided by the NASA Office of Space Science via grant NNX09AF08G and by other grants and contracts.

This publication uses VOSA, developed under the Spanish Virtual Observatory project supported from the Spanish MICINN through grant AyA2011-2.

The Digitized Sky Surveys were produced at the Space Telescope Science Institute under U.S. Government grant NAG W-2166. The images of these surveys are based on photographic data obtained using the Oschin Schmidt Telescope on Palomar Mountain and the UK Schmidt Telescope. The plates were processed into the present compressed digital form with the permission of these institutions.

This research has used the SIMBAD data base and the VizieR catalogue access tool, operated at CDS, Strasbourg, France.

Based on observations made with ESO Telescopes at the La Silla Observatory under programme ID 093.D-0431. We thank Javier Alarcón for operating the NTT. The INT is operated on the island of La Palma by the Isaac Newton Group in the Spanish Observatorio del Roque de los Muchachos of the Instituto de Astrofísica de Canarias. The IDS spectroscopy was obtained as part of I15AN007 and I/2015A/04. Based on observations collected at Copernico telescope (Asiago, Italy) of the INAF – Osservatorio Astronomico di Padova.

The research leading to these results has received funding from the European Research Council under the European Union's Seventh Framework Programme (FP/2007-2013)/ERC Grant Agreement no. 320964 (WDTracer). Support for this work was provided by NASA through Hubble Fellowship grant #HST-HF2-51357.001-A, awarded by the Space Telescope Science Institute, which is operated by the Association of Universities for Research in Astronomy, Incorporated, under NASA contract NAS5-26555.

REFERENCES

Allard F., Homeier D., Freytag B., Sharp C. M., 2012, in Reylé C., Charbonnel C., Schultheis M., eds, EAS Publ. Ser. Vol. 57, Low-Mass Stars and the Transition Stars/Brown Dwarfs. p. 3

Althaus L. G., Córsico A. H., Isern J., García-Berro E., 2010, A&AR, 18, 471

Baraffe I., Chabrier G., Allard F., Hauschildt P. H., 1998, A&A, 337, 403

Baraffe I., Chabrier G., Barman T. S., Allard F., Hauschildt P. H., 2003, A&A, 402, 701

Barentsen G. et al., 2014, MNRAS, 444, 3230

Becklin E. E., Zuckerman B., 1988, Nature, 336, 656

Bell K. J., Hermes J. J., Bischoff-Kim A., Moorhead S., Montgomery M. H., Østensen R., Castanheira B. G., Winget D. E., 2015, ApJ, 809, 14

Bell K. J. et al., 2016, ApJ, 829, 82

Bergeron P. et al., 2011, ApJ, 737, 28

Bianchi L., Efremova B., Herald J., Girardi L., Zabot A., Marigo P., Martin C., 2011, MNRAS, 411, 2770

Borucki W. J. et al., 2010, Science, 327, 977

Brown W. R., Kilic M., Allende Prieto C., Kenyon S. J., 2010, ApJ, 723, 1072

Brown W. R., Kilic M., Gianninas A., 2017, ApJ, 839, 23

Buzzoni B. et al., 1984, The Messenger, 38, 9

Camarota L., Holberg J. B., 2014, MNRAS, 438, 3111

Campante T. L. et al., 2016, ApJ, 830, 138
Catalán S., Isern J., García-Berro E., Ribas I., 2008, MNRAS, 387, 1693
Drew J. E. et al., 2014, MNRAS, 440, 2036
Dufour P., Blouin S., Coutu S., Fortin-Archambault M., Thibeault C., Bergeron P., Fontaine G., 2017, in Tremblay P.-E., Gaensicke B., Marsh T., eds, ASP Conf. Ser. Vol. 509, The Montreal White Dwarf Database: A Tool for the Community. Astron. Soc. Pac., San Francisco, p. 3
Faedi F., West R. G., Burleigh M. R., Goad M. R., Hebb L., 2011, MNRAS, 410, 899
Farihi J., Becklin E. E., Zuckerman B., 2005, ApJS, 161, 394
Fontaine G., Brassard P., 2008, PASP, 120, 1043
Fontaine G., Brassard P., Bergeron P., 2001, PASP, 113, 409
Gaia Collaboration, 2016a, A&A, 595, A1
Gaia Collaboration, 2016b, A&A, 595, A2
Gentile Fusillo N. P., Gänsicke B. T., Greiss S., 2015, MNRAS, 448, 2260
Gentile Fusillo N. P. et al., 2017, MNRAS, 469, 621
Giammichele N., Bergeron P., Dufour P., 2012, ApJS, 199, 29
Gianninas A., Bergeron P., Dupuis J., Ruiz M. T., 2010, ApJ, 720, 581
Gianninas A., Kilic M., Brown W. R., Canton P., Kenyon S. J., 2015, ApJ, 812, 167
Giclas H. L., Burnham Jr R., Thomas N. G., 1980, Lowell Obs. Bull., 8, 157
Girven J., Gänsicke B. T., Steeghs D., Koester D., 2011, MNRAS, 417, 1210
Green E. M. et al., 2015, in Dufour P., Bergeron P., Fontaine G., eds, ASP Conf. Ser. Vol. 493, High-speed Photometric Observations of ZZ Ceti White Dwarf Candidates. Astron. Soc. Pac., San Francisco, p. 237
Greiss S. et al., 2016, MNRAS, 457, 2855
Henden A., Munari U., 2014, Contrib. Astron. Obs. Skalnate Pleso, 43, 518
Henden A. A., Templeton M., Terrell D., Smith T. C., Levine S., Welch D., 2016, VizieR Online Data Catalog, 2336
Hermes J. J. et al., 2011, ApJ, 741, L16
Hermes J. J. et al., 2015, ApJ, 810, L5
Høg E. et al., 2000, A&A, 357, 367
Hogan E., Burleigh M. R., Clarke F. J., 2009, MNRAS, 396, 2074
Holberg J. B., Oswalt T. D., Sion E. M., McCook G. P., 2016, MNRAS, 462, 2295
Howell S. B. et al., 2014, PASP, 126, 398
Kawka A., Vennes S., 2006, ApJ, 643, 402
Kepler S. O., Giovannini O., Kanaan A., Wood M. A., Claver C. F., 1995, Balt. Astron., 4, 157
Kepler S. O. et al., 2015, MNRAS, 446, 4078
Kepler S. O. et al., 2016, MNRAS, 455, 3413
Kilic M. et al., 2006, AJ, 131, 582
Kilkenny D., O'Donoghue D., Koen C., Stobie R. S., Chen A., 1997, MNRAS, 287, 867
Kleinman S. J. et al., 2013, ApJS, 204, 5
Koester D., 2010, Mem. Soc. Astron. Ital., 81, 921
Koester D., Voss B., Napiwotzki R., Christlieb N., Homeier D., Lisker T., Reimers D., Heber U., 2009, A&A, 505, 441
Law N. M. et al., 2015, PASP, 127, 234
Lépine S., Shara M. M., 2005, AJ, 129, 1483
Limoges M.-M., Bergeron P., 2010, ApJ, 714, 1037
Limoges M.-M., Lépine S., Bergeron P., 2013, AJ, 145, 136
Limoges M.-M., Bergeron P., Lépine S., 2015, ApJS, 219, 19
Lindegren L. et al., 2016, A&A, 595, A4
McCook G. P., Sion E. M., 1999, ApJS, 121, 1
Marsh T. R., 1989, PASP, 101, 1032
Monet D. G. et al., 2003, AJ, 125, 984
Morrissey P. et al., 2007, ApJS, 173, 682
Munari U. et al., 2014, AJ, 148, 81
Napiwotzki R. et al., 2003, The Messenger, 112, 25
Napiwotzki R. et al., 2004, in Hilditch R. W., Hensberge H., Pavlovski K., eds, ASP Conf. Ser. Vol. 318, Spectroscopically and Spatially Resolving the Components of the Close Binary Stars. Astron. Soc. Pac., San Francisco, p. 402
O'Malley E. M., von Hippel T., van Dyk D. A., 2013, ApJ, 775, 1
Østensen R. H. et al., 2011, MNRAS, 414, 2860
Oswalt T. D., Smith J. A., Wood M. A., Hintzen P., 1996, Nature, 382, 692
Pauli E.-M., Napiwotzki R., Altmann M., Heber U., Odenkirchen M., Kerber F., 2003, A&A, 400, 877
Pickles A. J., 1998, PASP, 110, 863
Raddi R. et al., 2016, MNRAS, 457, 1988
Rebassa-Mansergas A., Nebot Gómez-Morán A., Schreiber M. R., Girven J., Gänsicke B. T., 2011, MNRAS, 413, 1121
Rebassa-Mansergas A., Nebot Gómez-Morán A., Schreiber M. R., Gänsicke B. T., Schwope A., Gallardo J., Koester D., 2012, MNRAS, 419, 806
Rebassa-Mansergas A., Ren J. J., Parsons S. G., Gänsicke B. T., Schreiber M. R., García-Berro E., Liu X.-W., Koester D., 2016, MNRAS, 458, 3808
Reid I. N., Sahu K. C., Hawley S. L., 2001, ApJ, 559, 942
Ricker G. R. et al., 2015, J. Astron. Telesc. Instrum. Syst., 1, 014003
Shanks T. et al., 2015, MNRAS, 451, 4238
Si S., van Dyk D. A., von Hippel T., Robinson E., Webster A., Stenning D., 2017, MNRAS, 468, 4374
Sion E. M., Holberg J. B., Oswalt T. D., McCook G. P., Wasatonic R., Myszka J., 2014, AJ, 147, 129
Skrutskie M. F. et al., 2006, AJ, 131, 1163
Steele P. R., Burleigh M. R., Dobbie P. D., Jameson R. F., Barstow M. A., Satterthwaite R. P., 2011, MNRAS, 416, 2768
Subasavage J. P., Jao W.-C., Henry T. J., Bergeron P., Dufour P., Ianna P. A., Costa E., Méndez R. A., 2009, AJ, 137, 4547
Taylor M. B., 2006, in Gabriel C., Arviset C., Ponz D., Enrique S., eds, ASP Conf. Ser. Vol. 351, Astronomical Data Analysis Software and Systems XV. Astron. Soc. Pac., San Francisco, p. 666
Tremblay P.-E., Bergeron P., 2009, ApJ, 696, 1755
Tremblay P.-E., Ludwig H.-G., Steffen M., Freytag B., 2013, A&A, 559, A104
Tremblay P.-E., Kalirai J. S., Soderblom D. R., Cignoni M., Cummings J., 2014, ApJ, 791, 92
Tremblay P.-E., Gianninas A., Kilic M., Ludwig H.-G., Steffen M., Freytag B., Hermes J. J., 2015, ApJ, 809, 148
Tremblay P.-E. et al., 2017, MNRAS, 465, 2849
van Leeuwen F., 2007, A&A, 474, 653
van Leeuwen F. et al., 2017, A&A, 599, A32
Vanderburg A. et al., 2015, Nature, 526, 546
Voss B., Koester D., Napiwotzki R., Christlieb N., Reimers D., 2007, A&A, 470, 1079
Wenger M. et al., 2000, A&AS, 143, 9
West R. G. et al., 2016, The Messenger, 165, 10
Winget D. E., Kepler S. O., 2008, ARA&A, 46, 157
Winget D. E., Hansen C. J., Liebert J., van Horn H. M., Fontaine G., Nather R. E., Kepler S. O., Lamb D. Q., 1987, ApJ, 315, L77
Wood M. A., 1992, ApJ, 386, 539
Wood M. A., 1995, in Koester D., Werner K., eds, Lecture Notes in Physics, Vol. 443, White Dwarfs. Springer-Verlag, Berlin, p. 41
Wright E. L. et al., 2010, AJ, 140, 1868
Zanutta A., Bianco A., Landoni M., Tomasella L., Benetti S., Giro E., 2014, in Ramsay S. K., McLean I. S., Takami H., eds, Proc. SPIE Conf. Ser. Vol. 9147, Ground-based and Airborne Instrumentation for Astronomy V. SPIE, Bellingham, p. 91474E
Zorotovic M., Schreiber M. R., 2013, A&A, 549, A95

SUPPORTING INFORMATION

Supplementary data are available at CDS via anonymous ftp to cdsarc.u-strasbg.fr (130.79.128.5) or via http://cdsarc.u-strasbg.fr/viz-bin/qcat?J/MNRAS

Table A1. Header of the online tables containing photometry and proper motions of white dwarfs we have presented in this work.

Please note: Oxford University Press is not responsible for the content or functionality of any supporting materials supplied by the authors. Any queries (other than missing material) should be directed to the corresponding author for the article.

APPENDIX A: ONLINE TABLES

Table A1. Header of the online tables containing photometry and proper motions of white dwarfs we have presented in this work.

APASS		Name based on APASS position
Names		Simbad names
ra_apass	deg	APASS Right Ascension
dec_apass	deg	APASS Declination
B	mag	APASS *B* magnitude
err_B	mag	APASS *B* magnitude error
V	mag	APASS *V* magnitude
err_V	mag	APASS *V* magnitude error
g	mag	APASS g' magnitude
err_g	mag	APASS g' magnitude error
r	mag	APASS r' magnitude
err_r	mag	APASS r' magnitude error
i	mag	APASS $'i$ magnitude
err_i	mag	APASS i' magnitude error
fuv	mag	*GALEX* FUV magnitude
err_fuv	mag	*GALEX* FUV magnitude error
nuv	mag	*GALEX* NUV magnitude
err_nuv	mag	*GALEX* NUV magnitude error
pmra	mas yr^{-1}	$\mu_\alpha \cos\delta$
err_pmra	mas yr^{-1}	$\mu_\alpha \cos\delta$ error
pmdec	mas yr^{-1}	μ_δ
err_pmdec	mas yr^{-1}	μ_δ error
J	mag	2MASS *J* magnitude
err_J	mag	2MASS *J* magnitude error
H	mag	2MASS *H* magnitude
err_H	mag	2MASS *H* magnitude error
K	mag	2MASS K_s magnitude
err_K	mag	2MASS K_s magnitude error
W1	mag	*WISE W*1 magnitude
err_W1	mag	*WISE W*1 magnitude error
W2	mag	*WISE W*2 magnitude
err_W2	mag	*WISE W*2 magnitude error

APPENDIX B: PHYSICAL PARAMETERS OF SPECTROSCOPICALLY CONFIRMED WHITE DWARFS

Table B1. Properties of the follow-up white dwarf sample. Columns are as follows: short name of the object, based on APASS coordinates; SIMBAD name, if known; telescope and observing date of spectrum used to assess the atmospheric parameters; effective temperature, surface gravity and the corresponding 3D corrections interpolated from the tables in Tremblay et al. (2013); masses and cooling ages, interpolated from Fontaine et al. (2001) cooling sequences; spectroscopic distances.

Short Name	SIMBAD	Telescope	Date	SpT	$T_{\rm eff}$ (K)	$\Delta T_{\rm 3D}$ (K)	$\log g$ (cgs)	$\Delta \log g_{\rm 3D}$ (cgs)	Mass ($M_\odot$)	$\tau_{\rm cool}$ (Gyr)	d (pc)
J0008+3645	GD 4	Copernico	2016/12/27	cZZ	12520 ± 620	−160	8.04 ± 0.14	−0.03	0.62 ± 0.05	0.37 ± 0.07	75 ± 3
J0018−0956	PHL 778	NTT	2014/06/15	DBA	16320 ± 100		8.00				
J0033+1021	2MASS J00335106+1021404	NTT	2014/07/12	DC	11640 ± 300		8.00				
J0106+3930	GD 10	Copernico	2016/11/07	DA	9830 ± 100	−130	8.39 ± 0.05	−0.27	0.68 ± 0.06	0.82 ± 0.13	38 ± 1
J0126−6556		NTT	2014/06/14	DA	13400 ± 340	50	8.18 ± 0.06	0.01	0.74 ± 0.06	0.38 ± 0.06	56 ± 2
J0128−6915		NTT	2014/06/14	DA	8720 ± 90	−30	8.18 ± 0.10	−0.25	0.56 ± 0.06	0.82 ± 0.12	49 ± 2
J0130+2638		NTT	2014/07/12	DA	13470 ± 400	50	8.25 ± 0.07	0.01	0.77 ± 0.06	0.41 ± 0.07	52 ± 2
J0130+5321	GD 278	Copernico	2016/12/30	DA	8840 ± 30		6.00 ± 0.00		0.16 ± 0.00	3.01 ± 0.09	138 ± 5
J0201+1212	GD 21	Copernico	2016/12/28	DC	7800 ± 200		8.00				
J0204+0726	GD 23	Copernico	2016/12/29	DA	18630 ± 1000		8.36 ± 0.13		0.84 ± 0.06	0.19 ± 0.05	98 ± 4
J0219−6306		NTT	2014/06/15	DAMS	9610 ± 600	−150	7.99 ± 0.32	−0.26	0.47 ± 0.05	0.53 ± 0.10	70 ± 4
J0220−0736	2MASS J02202493−0736271	NTT	2014/06/15	DAMS	12680 ± 260	−60	7.86 ± 0.06	−0.01	0.54 ± 0.05	0.27 ± 0.04	83 ± 3
J0242−8206		NTT	2014/06/15	DA	9200 ± 240	−60	8.67 ± 0.19	−0.28	0.85 ± 0.06	1.61 ± 0.29	47 ± 2
J0347+4358	Wolf 226	INT	2015/03/04	DA	13230 ± 190	90	7.94 ± 0.04		0.58 ± 0.05	0.26 ± 0.04	33 ± 1
J0421+4607		INT	2015/03/04	DA	7650 ± 50		8.00 ± 0.10	−0.14	0.53 ± 0.05	1.06 ± 0.13	27 ± 1
J0502+5401	LP 119−10	INT	2015/03/05	ZZ	11720 ± 220	−270	8.33 ± 0.04	−0.11	0.74 ± 0.06	0.61 ± 0.10	41 ± 2
J0510+2315		INT	2015/03/03	DAMS	22710 ± 820		8.32 ± 0.11		0.83 ± 0.06	0.09 ± 0.02	65 ± 3
J0515+5021	GD 289	INT	2015/03/05	DA	9520 ± 90	−120	8.26 ± 0.08	−0.26	0.60 ± 0.06	0.74 ± 0.12	37 ± 2

Table B1 – *continued*

Short Name	SIMBAD	Telescope	Date	SpT	$T_{\rm eff}$ (K)	$\Delta T_{\rm 3D}$ (K)	$\log g$ (cgs)	$\Delta\log g_{\rm 3D}$ (cgs)	Mass ($M_\odot$)	$\tau_{\rm cool}$ (Gyr)	d (pc)
J0529−0941		INT	2015/03/05	DA	14550 ± 370		8.26 ± 0.07		0.77 ± 0.06	0.33 ± 0.06	71 ± 3
J0603+4518		INT	2015/03/04	DA	16710 ± 290		7.85 ± 0.05		0.54 ± 0.05	0.11 ± 0.02	69 ± 3
J0634+3848	GD 260	INT	2015/03/04	cZZ	12610 ± 240	−300	8.50 ± 0.05	−0.05	0.89 ± 0.06	0.71 ± 0.12	49 ± 2
J0753+6122	GD 453	INT	2015/03/04	DC	9330 ± 230		8.00				
J0812+1737	GALEX J081237.8+173701	INT	2015/03/06	DA	16730 ± 140		7.95 ± 0.03		0.60 ± 0.05	0.13 ± 0.02	30 ± 1
J0823+7158	GD 458	INT	2015/03/04	DA	15300 ± 420		7.89 ± 0.07		0.56 ± 0.05	0.16 ± 0.03	88 ± 3
J0838−2146		INT	2015/03/05	DA	21990 ± 440		7.95 ± 0.07		0.61 ± 0.05	0.04 ± 0.01	85 ± 3
J0847−7312	WD 0848−730	NTT	2014/06/13	DA	17620 ± 610		7.98 ± 0.10		0.61 ± 0.05	0.11 ± 0.02	73 ± 3
J0857−2245		NTT	2014/06/13	DA	10730 ± 290	−240	7.95 ± 0.10	−0.18	0.49 ± 0.05	0.42 ± 0.05	50 ± 2
J0859−3124		NTT	2014/06/15	DA	31020 ± 650		8.34 ± 0.15		0.85 ± 0.06	0.03 ± 0.01	133 ± 6
J0900−0909		INT	2015/03/05	DA	21110 ± 320		7.80 ± 0.05		0.53 ± 0.04	0.04 ± 0.01	73 ± 3
J0905−2342		NTT	2014/06/15	DA	18270 ± 250		7.75 ± 0.05		0.51 ± 0.05	0.07 ± 0.01	98 ± 3
J0919+7723		INT	2015/03/06	DA	9160 ± 70	−100	7.91 ± 0.08	−0.27	0.43 ± 0.05	0.54 ± 0.06	41 ± 1
J1003−3145		NTT	2014/06/14	DAMS	13560 ± 750	130	7.95 ± 0.08	0.02	0.60 ± 0.05	0.26 ± 0.06	116 ± 5
J1003−0337	GD 110	NTT	2014/06/14	DA	8420 ± 50	−20	8.06 ± 0.07	−0.23	0.51 ± 0.05	0.79 ± 0.08	37 ± 1
J1010−2427		INT	2015/03/06	DC	20370 ± 300		8.00				
J1021−3448		NTT	2014/07/13	DA	13240 ± 720	80	8.04 ± 0.12		0.64 ± 0.06	0.31 ± 0.07	81 ± 3
J1022−3226		NTT	2014/07/13	DAMS	60180 ± 5270		7.77 ± 0.34		0.63 ± 0.04	0.00 ± 0.00	288 ± 14
J1040−3123		NTT	2014/06/15	DA	8270 ± 100	−10	8.15 ± 0.12	−0.2	0.57 ± 0.05	0.95 ± 0.13	48 ± 2
J1052−1137		NTT	2014/06/15	DA	18520 ± 350		7.83 ± 0.06		0.55 ± 0.05	0.08 ± 0.01	145 ± 5
J1058+5132		INT	2015/03/03	cZZ	12320 ± 640	−230	8.07 ± 0.12	−0.04	0.63 ± 0.05	0.40 ± 0.08	88 ± 4
J1128+5919	SDSS J112805.30+591957.9	INT	2015/03/03	DA	14890 ± 670		7.58 ± 0.15		0.41 ± 0.04	0.12 ± 0.02	140 ± 5
J1131−1225		NTT	2014/06/13	cZZ	12160 ± 420	−280	8.20 ± 0.09	−0.06	0.69 ± 0.06	0.48 ± 0.09	51 ± 2
J1142−1803	EC 11396-1746	INT	2015/05/13	DA	8860 ± 140		6.76 ± 0.28		0.21 ± 0.02	1.16 ± 0.44	115 ± 6
J1212−3642		NTT	2014/07/12	DA	20150 ± 360		7.75 ± 0.05		0.51 ± 0.04	0.05 ± 0.01	90 ± 3
J1223−1852	EC 12206-1835	INT	2015/03/05	DC	10660 ± 300		8.00				
J1229−0432	LP 675-43	NTT	2014/07/12	DC	9950 ± 400		8.00				
J1254−3856		NTT	2014/06/15	DA	13030 ± 330	40	8.01 ± 0.08	−0.01	0.61 ± 0.05	0.30 ± 0.05	87 ± 3
J1331+6809	GD 487	Copernico	2016/12/29	DA	10750 ± 250	−130	9.00 ± 0.14	−0.2	1.08 ± 0.05	1.71 ± 0.21	36 ± 2
J1342−1413		NTT	2014/06/15	DA	13870 ± 410	−70	8.64 ± 0.06	0.01	1.01 ± 0.06	0.75 ± 0.15	51 ± 2
J1401−0553		NTT	2014/07/12	DA	15930 ± 860		7.92 ± 0.11		0.58 ± 0.05	0.15 ± 0.04	107 ± 4
J1402−0736	SDSS J140233.97−073650.6	NTT	2014/06/15	DA	8590 ± 100	−10	8.51 ± 0.10	−0.23	0.78 ± 0.06	1.56 ± 0.29	51 ± 2
J1407−0626		INT	2015/03/03	DA	8390 ± 70	−10	8.24 ± 0.10	−0.22	0.62 ± 0.06	1.04 ± 0.17	25 ± 1
J1418+0929	2MASS J14183529+0929195	INT	2015/05/13	DA	17150 ± 290		7.84 ± 0.06		0.55 ± 0.05	0.10 ± 0.02	104 ± 4
J1420−2457	2MASS J14200652−2457026	NTT	2014/06/14	DAMS	13530 ± 1020	90	8.17 ± 0.14	0.01	0.72 ± 0.06	0.36 ± 0.09	104 ± 4
J1438−3127		NTT	2014/06/13	DAMS	14520 ± 510		7.44 ± 0.09		0.36 ± 0.03	0.10 ± 0.02	75 ± 3
J1455+5655	SBSS 1453+571	INT	2015/03/04	DA	15230 ± 520		7.97 ± 0.06		0.60 ± 0.05	0.19 ± 0.03	53 ± 2
J1517+1030	SDSS J151754.62+103044.3	NTT	2014/06/13	DA	19920 ± 600		7.86 ± 0.10		0.56 ± 0.05	0.06 ± 0.01	122 ± 5
J1528−2515		NTT	2014/06/13	DA	14960 ± 370		8.40 ± 0.08		0.86 ± 0.06	0.38 ± 0.07	49 ± 2
J1549−3954		NTT	2014/07/12	DB	12760 ± 200		8.00				
J1614+1046		NTT	2014/06/13	DA	16800 ± 970		8.03 ± 0.12		0.64 ± 0.06	0.15 ± 0.04	95 ± 4
J1620−1901		NTT	2014/06/15	DA	13920 ± 160	10	8.35 ± 0.04	0.01	0.84 ± 0.06	0.44 ± 0.07	47 ± 2
J1638−2035		INT	2015/05/13	DA	8480 ± 110	−10	8.28 ± 0.14	−0.23	0.63 ± 0.06	1.05 ± 0.19	40 ± 1
J1700−8723		NTT	2014/06/14	cZZ	10900 ± 350	−230	8.20 ± 0.08	−0.18	0.62 ± 0.05	0.54 ± 0.09	33 ± 1
J1729+0208		INT	2015/05/13	DA	15460 ± 760		7.85 ± 0.09		0.55 ± 0.05	0.15 ± 0.03	113 ± 4
J1730+1346	GD 208	INT	2015/05/13	DA	10500 ± 180	−200	8.27 ± 0.05	−0.25	0.62 ± 0.06	0.59 ± 0.09	39 ± 1
J1944−3603		NTT	2014/06/15	DA	12970 ± 150	10	8.03 ± 0.03	−0.01	0.63 ± 0.05	0.32 ± 0.04	30 ± 1
J1956+6413		INT	2015/05/13	DA	17780 ± 480		7.81 ± 0.09		0.53 ± 0.05	0.09 ± 0.02	81 ± 4
J2017−1712		INT	2015/05/14	DA	42800 ± 840		7.97 ± 0.09		0.67 ± 0.05	0.00 ± 0.00	103 ± 4
J2023−1115		INT	2015/05/15	DA	16620 ± 310		8.04 ± 0.04		0.64 ± 0.06	0.15 ± 0.03	51 ± 2
J2025+7900		INT	2015/05/16	DA	24030 ± 460		8.06 ± 0.06		0.67 ± 0.06	0.03 ± 0.01	113 ± 4
J2047−1259	EC 20444−1310	INT	2015/05/15	DAB	18630 ± 360		8.37 ± 0.06		0.85 ± 0.06	0.20 ± 0.04	80 ± 3
J2101−0527	SDSS J210110.16−052751.2	INT	2015/05/16	DBA	50530 ± 800		8.00				
J2109+6507		INT	2015/05/17	DAH	18220 ± 500		8.00				
J2112−2922	EC 21096−2934	NTT	2014/06/14	DC	10550 ± 110		8.00				
J2151−0502	HE 2149−0516	NTT	2014/06/14	DBA	12240 ± 30		8.00				
J2202+3848	GD 399	Copernico	2016/12/30	DA	9270 ± 60	−100	8.04 ± 0.09	−0.27	0.49 ± 0.05	0.60 ± 0.07	57 ± 2
J2221−0408	LP 700−3/4	NTT	2014/06/14	DAMS	9940 ± 830	−100	8.74 ± 0.36	−0.29	0.89 ± 0.06	1.46 ± 0.45	44 ± 3
J2228−3105	HE 2149−0516	NTT	2014/06/15	cZZ	12200 ± 220	−260	8.02 ± 0.06	−0.04	0.60 ± 0.05	0.38 ± 0.05	60 ± 2
J2233+2610	PM J22331+2610	INT	2015/05/18	DA	13430 ± 760	140	8.02 ± 0.09	0.02	0.64 ± 0.06	0.30 ± 0.07	67 ± 3
J2256−1319	PB 7361	NTT	2014/06/14	DA	20080 ± 400		7.97 ± 0.05		0.62 ± 0.05	0.07 ± 0.01	98 ± 4
J2308+0658	SDSS J230813.05+065836.8	NTT	2014/07/12	DAMS	34640 ± 250		7.80 ± 0.05		0.58 ± 0.04	0.01 ± 0.00	147 ± 6
J2331−6656	2MASS J23314533−6656078	NTT	2014/06/14	DA	7430 ± 60	10	7.86 ± 0.10	−0.13	0.46 ± 0.05	0.98 ± 0.10	43 ± 1
J2341+2924		NTT	2014/07/12	DA	13120 ± 230	10	8.10 ± 0.05	−0.01	0.67 ± 0.06	0.34 ± 0.05	64 ± 3

This paper has been typeset from a TEX/LATEX file prepared by the author.